Geoscience Frontiers 6 (2015) 227–246

HOSTED BY

Contents lists available at ScienceDirect

China University of Geosciences (Beijing)

Geoscience Frontiers

journal homepage: www.elsevier.com/locate/gsf

Research paper

Large-scale thrusting at the northern Junggar Basin since Cretaceous and its implications for the rejuvenation of the Central Asian Orogenic Belt

Jieyun Tang [a,b], Dengfa He [a,*], Di Li [a], Delong Ma [a]

[a] The Key Laboratory of Marine Reservoir Evolution and Hydrocarbon Accumulation Mechanism, The Ministry of Education, China University of Geosciences (Beijing), Beijing 100083, China
[b] Liaohe Oilfield Company, China National Petroleum Corporation, Panjin 124010, Liaoning, China

ARTICLE INFO

Article history:
Received 7 August 2013
Received in revised form
9 July 2014
Accepted 15 July 2014
Available online 12 August 2014

Keywords:
Mesozoic–Cenozoic
Thrust reactivity
Wulungu depression
Central Asian Orogenic Belt (CAOB)

ABSTRACT

The Wulungu Depression is the northernmost first-order tectonic unit in the Junggar Basin. It can be divided into three sub-units: the Hongyan step-fault zone, the Suosuoquan sag and the Wulungu south slope. The Cenozoic strata in the basin are intact and Mesozoic–Cenozoic deformation can be observed in the Wulungu step-fault zone, so this is an ideal place to study the Mesozoic–Cenozoic deformation. By integration of fault-related folding theories, regional geology and drilling data, the strata of the Cretaceous–Paleogene systems are divided into small layers which are selected as the subjects of this research. The combination of the developing unconformity with existing growth strata makes it conceivable that faults on the step-fault zone have experienced different degrees of reactivation of movement since the Cretaceous. Evolutionary analyses of the small layers using 2D-Move software showed certain differences in the reactivation of different segments of the Wulungu Depression such as the timing of reactivation of thrusting, for which the reactivity time of the eastern segment was late compared with those of the western and middle segments. In addition the resurrection strength was similarly slightly different, with the shortening rate being higher in the western segment than in the other segments. Moreover, the thrust fault mechanism is basement-involved combined with triangle shear fold, for which a forward evolution model was proposed.

1. Introduction

The Central Asian Orogenic Belt (CAOB) is a giant accretionary orogen between the European, Siberian, Tarim and North China cratons (Şengör et al., 1993; Jahn, 2004; Xiao et al., 2010) and is the most important area of Phanerozoic continental growth around the world (Şengör et al., 1993; Jahn et al., 2000; Kovalenko et al., 2004; Kröner et al., 2007, 2014; Safonova et al., 2009, 2011; Xiao et al., 2009, 2013, 2014; Li et al., 2013; Xiao and Santosh, 2014). It is widely accepted that the CAOB resulted from complicated accretion–collision processes involving Precambrian micro-continents, island arcs, seamounts, accretionary complexes and ophiolites during the evolution of the Paleo-Asian Ocean from the late Mesoproterozoic to the Mesozoic (Jahn, 2004; Windley et al., 2007; Xiao and Kusky, 2009; Xiao et al., 2010).

CAOB collision events had ceased by the end of the late Paleozoic, signalling the intra-plate evolution stage. The Paleozoic rocks were involved into the Mesozoic–Cenozoic deformation events (De Grave et al., 2007b); the Altay-Sayan experienced Jurassic–Cretaceous large-scale denudation, and as a result kilometres thick clastic sediments were accumulated in the intermountain basin (Howard et al., 2003). During the late Cretaceous–early Paleogene, the Altai experienced widespread peneplanation (Dobretsov et al., 1996; De Grave et al., 2007a,b, 2009). This period of peneplanation affected the entire CAOB, albeit somewhat earlier in the Gobi-Altai and Tianshan (Jolivet et al., 2007, 2010; Vassallo et al., 2007), to the south of the Altai. Mesozoic–Cenozoic basalt is widely distributed in several different parts of the central Asian region.

* Corresponding author. Tel.: +86 10 82323868; fax: +86 10 82326850.
E-mail addresses: hedengfa282@263.net, xdlidi@163.com (D. He).

Peer-review under responsibility of China University of Geosciences (Beijing).

http://dx.doi.org/10.1016/j.gsf.2014.07.003

However there are still controversies regarding the tectonic deformations during the Mesozoic–Cenozoic. There are many unresolved questions, for example, were the early faults reactive? What are the features of the reactivation? Furthermore, are the deformations continuous or staged? Chen et al. (2011) proposed that the Cenozoic tectonics of North Junggar involved reactivation of early deep-seated thrusts, resulting in extensional fractures and formation of many small depressions at the shallow crustal level. However, although this research attempted to describe the formation of the shallow depressions, there was little kinematic analysis of the deep early faults, and there was no reference to the late Mesozoic.

The Junggar Basin (JB) of northwestern China is located in the southwestern CAOB (Windley et al., 2007; Choulet et al., 2011; Xiao et al., 2013) (Fig. 1a and b). The northern Junggar Basin is bounded by the Kelameili Mountains to the southeast and the Qinggelidi Mountains to the northeast (Fig. 1c). The Cenozoic strata in the basin are intact and Mesozoic–Cenozoic deformation can be observed in the Wulungu step-fault zone. Therefore it is an ideal place to study this deformation.

2. Geological setting

2.1. Tectonic position

The northern margin of the Junggar Basin was an active tectonic belt during the Paleozoic (Coleman, 1989; Zhang et al., 2008; Zhang and Guo, 2010). The ancient Junggar Ocean, crossing the northern Xinjiang region, existed between the Siberian plate and the Kazakhstan plate. The ophiolite belt, outcropped in the northern margin of the Junggar Basin, has preserved information about the evolution of the ancient oceans (Jian et al., 2003; Zhang et al., 2003;

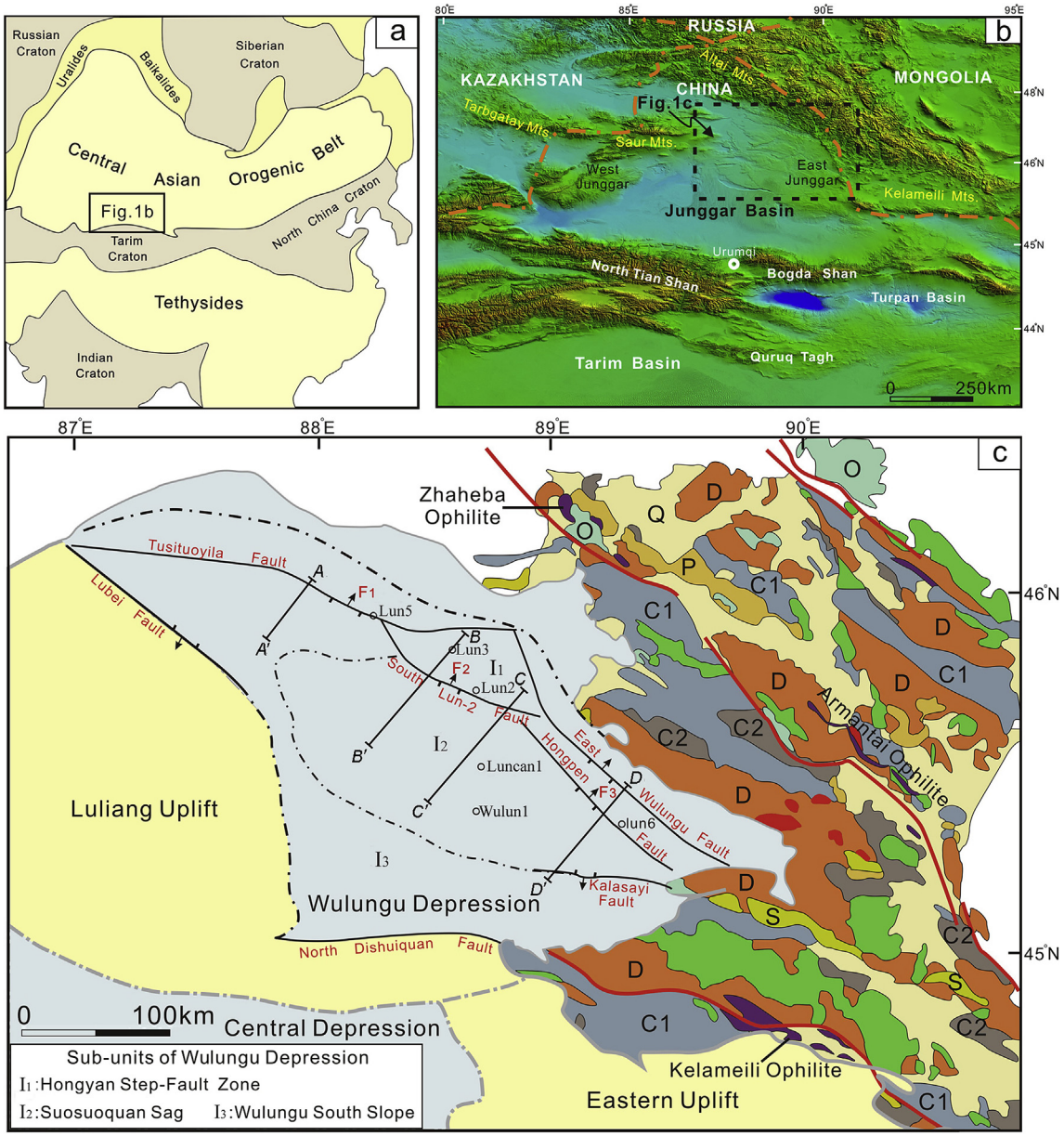

Figure 1. (a) Location of the study area in the Central Asian Orogenic Belt (modified from Ma et al., 2012); (b) Topographic map showing the location of the East Junggar in the Central Asian Orogenic Belt; (c) Geological map of the northern Junggar terrane. C1–Lower Carboniferous, C2–Upper Carboniferous, D–Devonian, S–Silurian, P–Permian, Q–Quaternary, O–Ordovician.

Xiao et al., 2006; Tang et al., 2007). Three ophiolite belts are distributed in the northeastern part of the basin. From north to south, these are the Kurt ophiolite belt, the Armantai ophiolite belt (Xiao et al., 2006, 2009) and the Kelameili ophiolite belt (Fig. 1c). The Kelameili ophiolite belt, along with the Da'erbute ophiolite belt in the western Junggar, represents the ancient Junggar Ocean (Ping et al., 2005; Tang et al., 2007; Wang et al., 2009). The Zhaheba ophiolite belt corresponds to a marginal basin or the back-arc basin and the Kuert ophiolite belt represents a back-arc basin to the north of the Junggar Ocean (Zhang et al., 2003; Shen et al., 2013). The suture zone closed completely at the end of the Carboniferous. The Yemaquan arc zone and the Kelameili suture can be tracked in the residual magnetic anomaly map of the northern margin of the Junggar Basin (Fig. 2a and b).

2.2. Tectonic units

The Wulungu Depression can be divided into three sub-units (Ren, 2008): the Hongyan step-fault zone; the Suosuoquan sag and the Wulungu south slope (Fig. 1c).

The Hongyan step-fault zone, which in the form of a ladder inclined to the south, is connected with the Wulungu north uplift belt in the north and the Suosuoquan sag in the south. The boundaries between them are faults: the Tuzituoyila Fault (F_1), the Wulungu north Fault (F_4), the Well Lun-2 south Fault (F_2) and the Bai'erkuduke Fault. The northwest trending pan-like Suosuoquan sag is connected with the Wulungu south slope in the south by the Kalasayi Fault (F_6). The sag was formed during the late Triassic (Ren, 2008). To the south of the Wulungu south slope is the Luliang Uplift, the boundaries between the two are the Lubei Fault (F_5) and the Dishuiquan north Fault (F_7). During the Mesozoic–Cenozoic the boundary between the Wulungu Depression and the Luliang Uplift moved southwards relative to its position during the Paleozoic era (Ren, 2008).

2.3. Stratigraphy

Paleozoic strata mainly crop out in the peripheral part of northern margin of the Junggar Basin, in which there are also occasional outcrops of Cenozoic strata (Fig. 1c). The deepest drilling well in the Suosuoquan sag is Well Wucan-1, which was drilled into clastic rock of lower Carboniferous, while other wells only drilled the upper Carboniferous. The only drilled Paleozoic strata are Carboniferous, and are mainly a series of volcanic rocks: the top is predominantly made up of tuff, with a few breccias, and the bottom is composed of tuffaceous shale. A large-scale regional unconformity exists between Paleozoic and Mesozoic strata, corresponding to Hercynian movements. Permian rocks are absent over the entire area. The development of the Triassic is not complete: only the upper Triassic is drilled in the Hongyan step-fault zone, while the Triassic developed relatively intact on the Suosuoquan sag, the Triassic is mainly made up of lacustrine clastic rock, containing some coal sandwich. Jurassic formations are coal measures strata (Fig. 3). A large-scale diachronic unconformity surface is present between the Jurassic and the Cretaceous strata. The unconformity corresponds to the second-phase Yanshan movement. The Cretaceous strata are predominantly of the Tugulu Group: brown mudstone and silty mudstone interbedded with minor siltstone

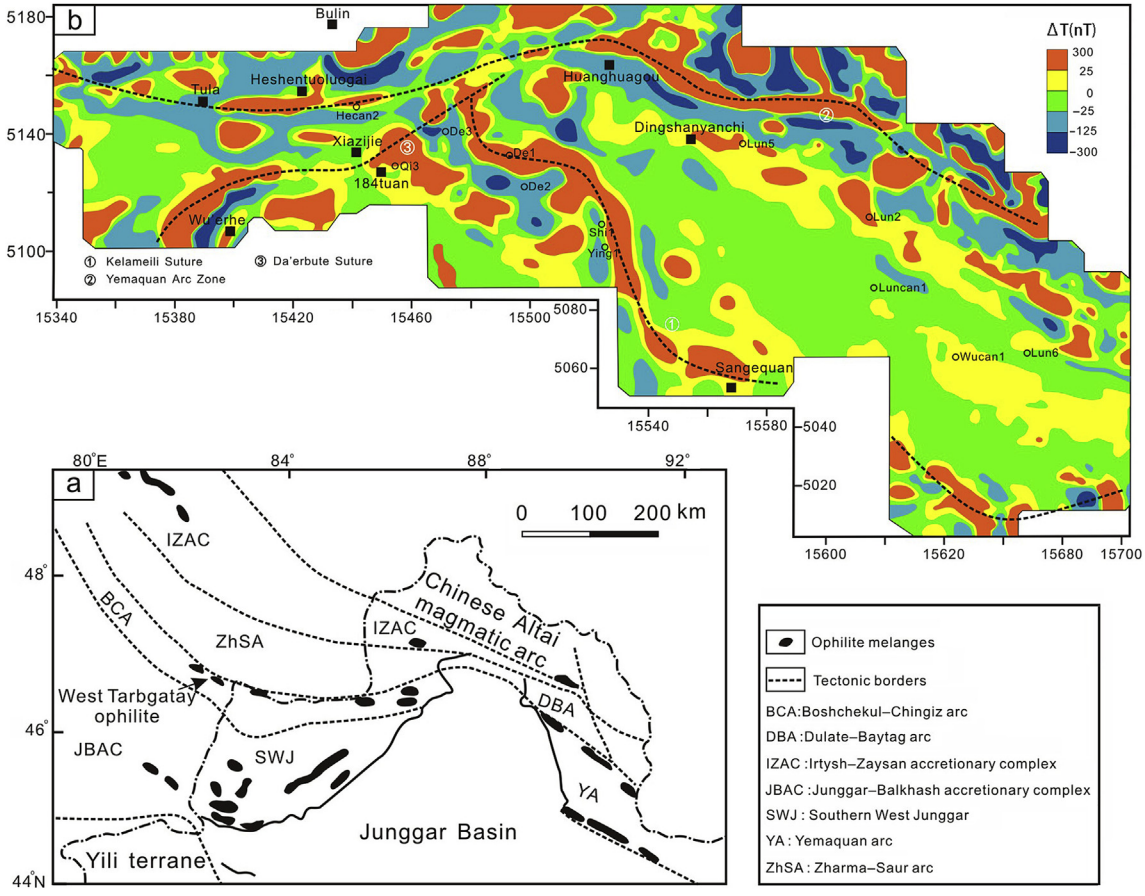

Figure 2. (a) Simplified tectonic framework of Northern Xinjiang; (b) Residual magnetic anomaly at the northern margin of the Junggar Basin.

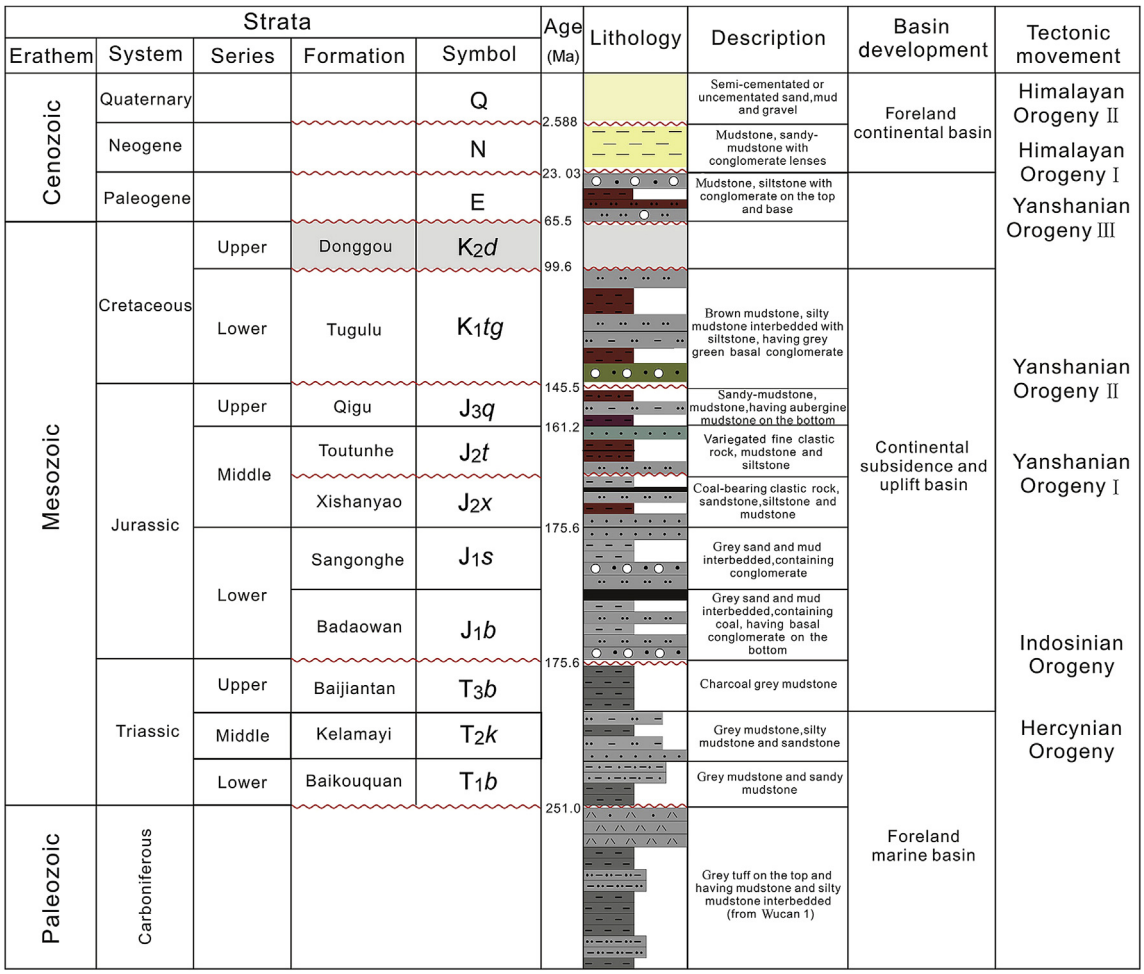

Figure 3. Comprehensive stratigraphical column of the Wulungu Depression.

and having a pale green basal conglomerate at the deepest point of the group (Fig. 3). The Cretaceous layers are in unconformable contact with the Paleogene (Fig. 4d). The Paleogene formations contain some mudstone and siltstone, with sandy conglomerate at the base and the top. The Neogene strata are mainly mudstone and sandy mudstone, containing conglomerate lenses. The base of the Neogene is a regionally diachronous unconformity surface.

3. Methods and database

Deposition in active tectonic settings is always controlled by growing structures at different scales. The inherent synchroneity of growth strata and coupled folding or faulting activity makes growth strata crucial to interpret fold-and-thrust geometry and kinematics (Suppe et al., 1992; Anastasio et al., 1997). Good examples of growth strata have been documented in the Pyrenees and the Ebro Basin (Anadón et al., 1986; Riba, 1989), the Alps (Lickorish and Ford, 1998), and the Apennines (Zoetemeijer et al., 1992; Butler and Lickorish, 1997). The western boundary of North and South America also provides significant examples of growth strata, such as in the Transverse Ranges in California (Medwedeff, 1989; Hummon et al., 1994; Shaw and Suppe, 1994; Souter and Hager, 1997), and the frontal Andes in Argentina (Zapata and Allmendinger, 1996). Precise studies of the geometries and sedimentological characteristics of growth strata associated with a particular structure are the key to understanding the kinematics of folding and faulting and the timing of deformation (Mascle et al., 1998).

The stages of deformation, as indicated by extensive angular unconformities, resulted in significant changes in the tectonic geomorphology and geography of the basin (Lin et al., 2012). The development of unconformities, particularly their erosion and origin within the dynamic setting of a basin, has been an important and long-term controversy in basin analysis. The formation of stratigraphic unconformities can be attributed to tectonics, eustasy, or climatic change (Huuse and Clausen, 2001; Dickinson et al., 2002; Jaimes and de De Freitas, 2006; Otonicar, 2007; Baranoski et al., 2009). However, angular unconformities with underlying deformed strata are usually generated by tectonic events or uplift (Coakley et al., 1991; Mindszenty et al., 1995; Paola and Domenico, 1995; Yu and Chou, 2001; Rafini et al., 2002; Li et al., 2004; Ghiglione and Ramos, 2005).

The northern Junggar Basin has been imaged by many 2D seismic reflection profiles which can reveal the structural deformation. In addition, many wells have been drilled in the Wulungu Depression: Wells Lun2, Lun3, Lun5 and Lun6 were drilled in the Hongyan step-fault zone, and Wells Luncan1, Lun7, Lun8 and Wucan1 are located in the Suosuoquan sag. All the wells can be incorporated in the horizon calibration of seismic data. This study uses an integrated database that includes distributed seismic profiles, well logs, and outcrop sections. Comprehensive analysis of 20 2D seismic profiles across the Wulungu Depression provides a firm basis for the recognition of the major angular unconformities. The

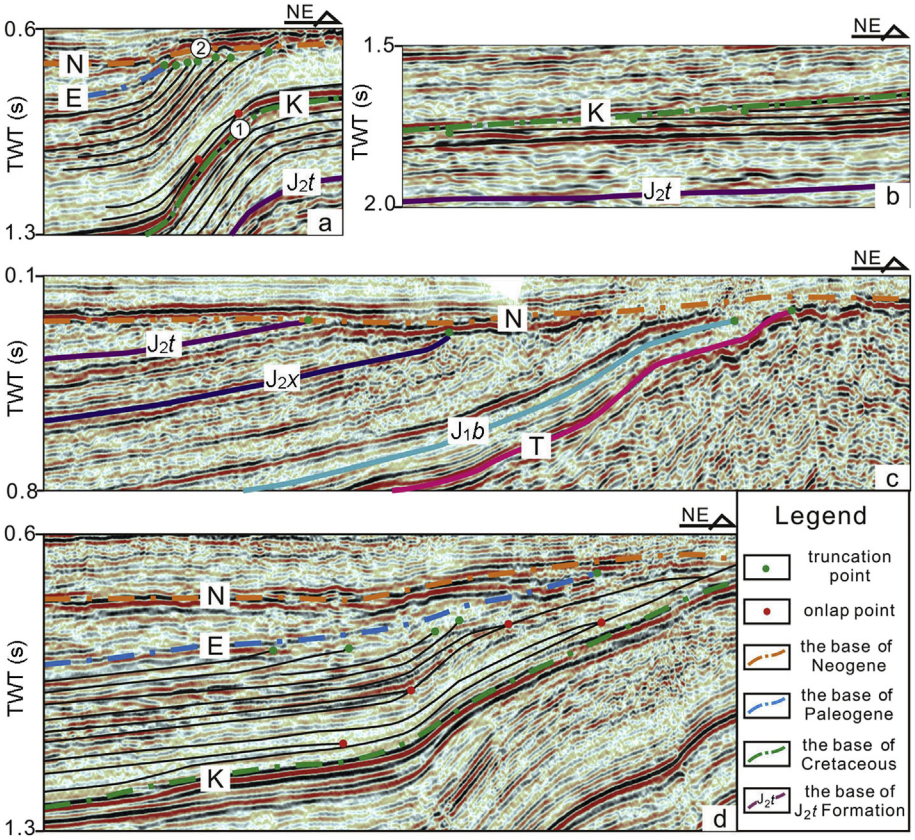

Figure 4. (a) ① Angular unconformity between the Jurassic and the Cretaceous, ② Angular unconformity between the Cretaceous and the Neogene (the green point indicates the truncation, the red point indicates onlap); (b) Angular unconformity between the Jurassic and the Cretaceous from the *B*–*B*′ profile (the green point indicates the truncation); (c) Angular unconformity between the Jurassic, the Triassic and the Neogene from the *B*–*B*′ profile; (d) Angular unconformity between the Paleogene and the Cretaceous (the green point indicates the truncation, the red point indicates onlap) from the *C*–*C*′ profile.

angular unconformities can be related to the major tectonic events or uplifts (Ghiglione and Ramos, 2005), and can then be used to determine the movement times of major tectonic events or uplifts. Accurate analysis of growth strata has revealed their significance for unravelling both fold kinematics and the timing of deformation in both compressive and extensive settings. This study uses analysis of growth strata in profiles to better study the growth structures and indicate the deformation times of the major faults along the Hongyan step-fault zone.

This study shows that multiple overlap points exist within the Cretaceous–Paleogene strata. The width between the overlap seismic events above the base of Cretaceous increases from the edge to the interior of the basin. This is a product of divergent overlap, which is not only caused by the sea-level change and tectonic subsidence, but also corresponds to tectonic deformation resulted from the activity of the faults. These kinds of overlap points can, to a certain extent, reflect the dynamic balance relationship between the tectonic activity rate and deposition rate.

In order to resolve the folding kinematics and study the comprehensive movement information of the faults, balanced cross-section construction, unfolding techniques and forward modelling techniques (e.g., Mount et al., 1990; Novoa et al., 2000) are needed. In this study, strata in the Cretaceous–Paleogene system are divided into small layers corresponding to events. By using 2D-Move software, evolutionary analysis of these small layers can be performed, from which we can draw conclusions about the characteristics of deformations since the Cretaceous.

By integrating fault-related folding theories, regional geology and drilling data, four typical profiles are selected and presented in this paper.

4. Analyses of seismic profiles

4.1. Characteristics of unconformities

The Wulungu region has developed three large regional unconformities since the Cretaceous. A large-scale diachronous unconformity surface occurs between the Jurassic and the Cretaceous strata, and this surface has a strong-amplitude continuous reflection axis on the seismic profile (Fig. 4a and b). In addition, obvious truncation points can be seen under the unconformity surface (Fig. 4b), as well as overlap points above the unconformity surface (Fig. 4a). The unconformity corresponds to the second-phase Yanshan movement. The Cretaceous strata are in unconformable contact with the Paleogene strata (Fig. 4d); this unconformity is visible in the seismic profile as a middle-strong amplitude and continuous reflection axis (Fig. 4d). Obvious truncation points can be seen under the reflection axis. The base of the Neogene is a regionally diachronous unconformity surface, with different contact relationships from the Suosuoquan sag to the step-fault zone from south to north: the Neogene unconformity overlies the Paleogene in the Suosuoquan sag (Fig. 4a); in the transition zone between the sag and step-fault zone, the Neogene cover on the Cretaceous strata with angle unconformity contact relationship. On the step-fault zone, the Neogene are successively angled unconformable contact with Jurassic and Triassic (Fig. 4c).

4.2. Characteristics of the sequence structure

The four survey lines chosen by this research cover the west, middle and east segments of the Wulungu Depression. The four

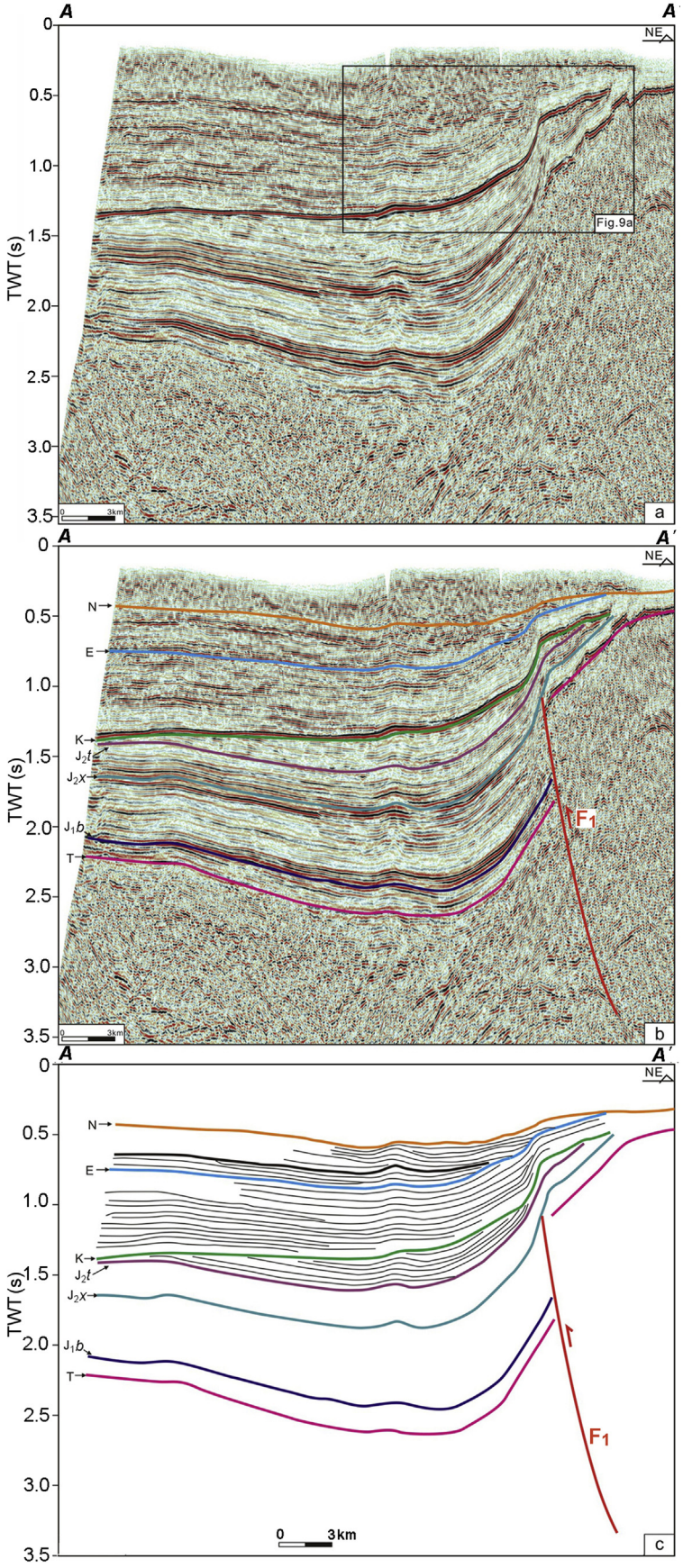

Figure 5. Seismic profile of *A*–*A*′. (a) Original profile of *A*–*A*′; (b) Interpreted profile of *A*–*A*′; (c) Pure interpreted profile of *A*–*A*′.

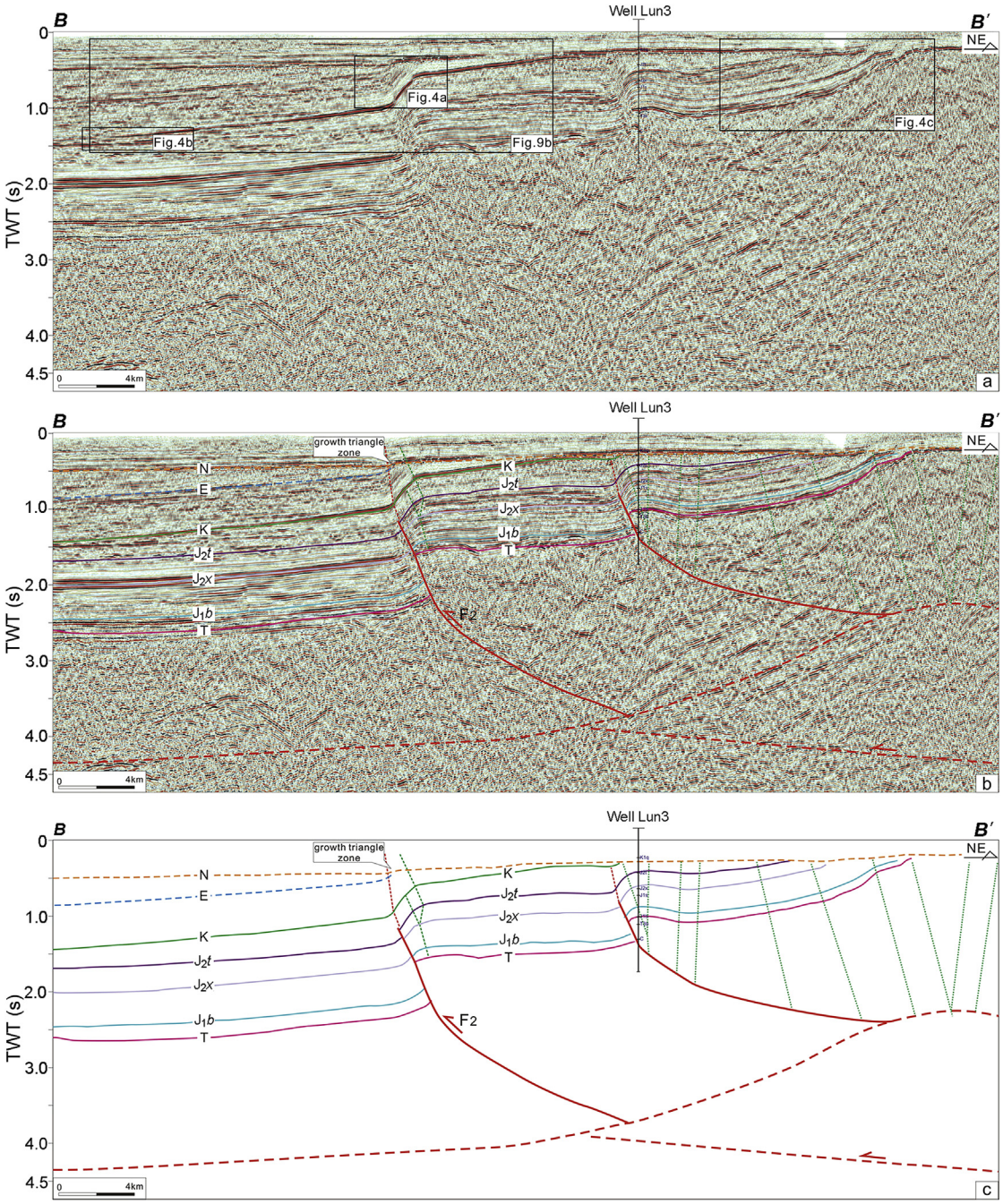

Figure 6. Seismic profile of *B*–*B*′. (a) Original profile of *B*–*B*′; (b) Interpreted profile of *B*–*B*′; (c) Pure interpreted profile of *B*–*B*′.

profiles are similar in structure (Figs. 5–8). The profiles are divided into the Suosuoquan sag and the Hongyan step-fault zone by the sag-controlled faults. In the west segment the Tuzituoyila fault is the sag-controlled fault, while in the middle and east they are the South Lun-2 Fault and the Hongpen Fault, respectively. In the *A*–*A*′ profile from the west segment (Fig. 5), the fault plane of the Tuzituoyila Fault is northeastward, with a steep upward angle. In the middle segment of the Wulungu Depression (Figs. 6 and 7), it is easy to recognize two sets of structural layers in the deep, structural wedge at the bottom and an imbricate structure at the top, separated by a detachment surface (Figs. 6 and 7). In the top imbricate structure, imbricate distributed faults, including the South Lun-2 Fault (F_2), converge at the lower detachment layer, and the faults became steeper with decreasing of depth. In addition, the *C*–*C*′ profile in the middle segment has already developed into antithetic faults, which meet the major fault in a Y-shape (Fig. 7). An analysis of the sag-controlled fault indicated that the folds that have resulted from the sag-controlled fault are asymmetrical and their fore-limbs are generally much steeper and narrower than their corresponding back-limbs. The fault displacement becomes smaller from the Triassic to the Jurassic strata, becoming zero at the endpoint. From these characteristics, we believe that the sag-controlled fault is a typical fault-propagation fold (Suppe and Medwedeff, 1990).

The Wulungu Depression lacks Permian sedimentary rocks entirely (Fig. 2) and there was no deposition in this area until the

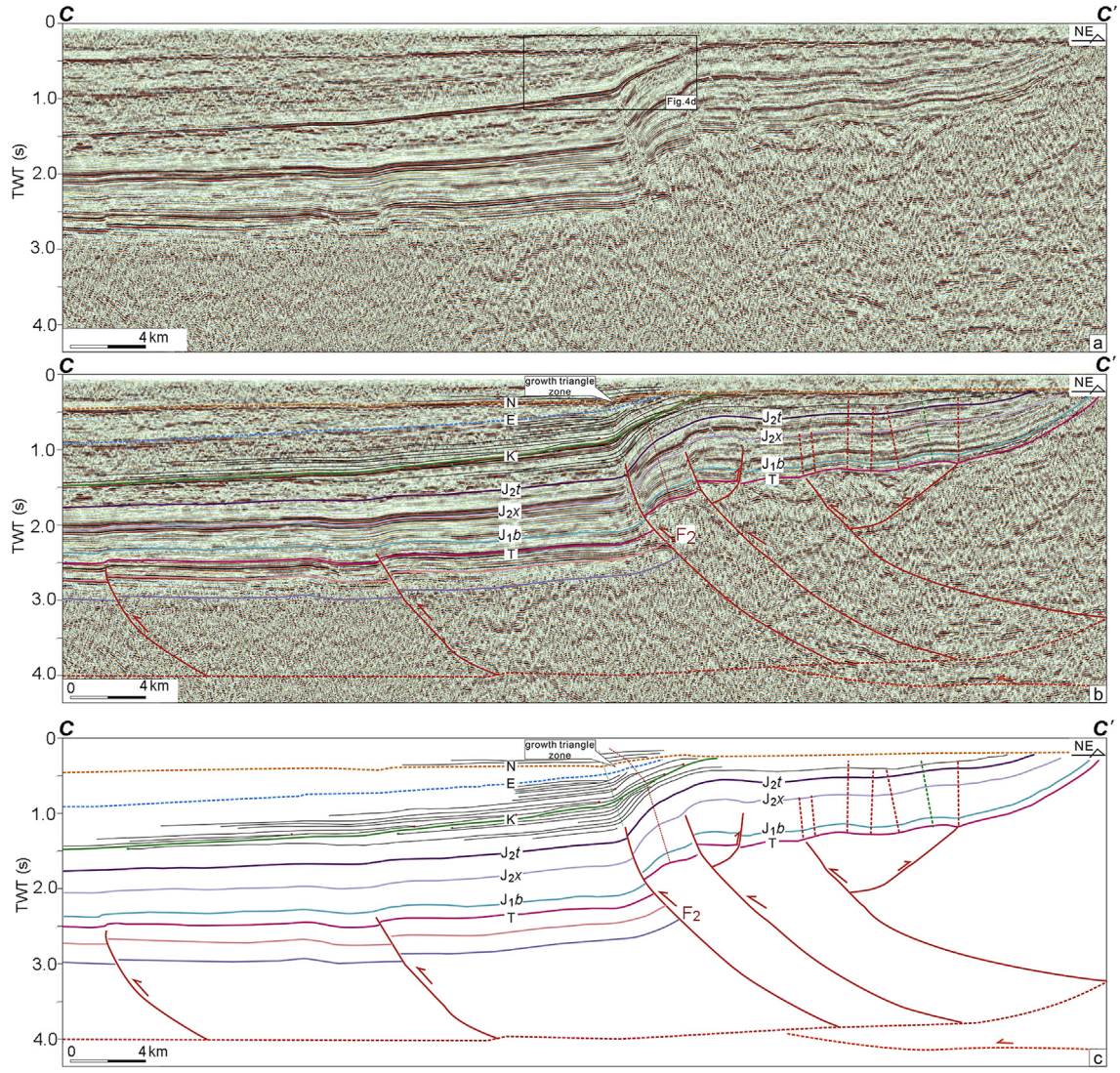

Figure 7. Seismic profile of *C*–*C*′. (a) Original profile of *C*–*C*′; (b) Interpreted profile of *C*–*C*′; (c) Pure interpreted profile of *C*–*C*′.

early Triassic. With the expansion of the lake domain in the late Triassic Junggar area, the entire basin was covered by water, with the Wulungu Depression acting as a sink for deposits (Ren, 2008). An analysis of the formation thickness up into the Triassic indicates that before the deposition of the Cretaceous rocks the sedimentary centre of the depression was located in the northernmost region of the Suosuoquan sag, close to the Hongyan fault terrace in the middle and west profiles (Figs. 5–7). At the beginning of the Cretaceous, the sedimentary centre migrated to the southwest. However, in the eastern profile (Fig. 8), as the width of the Suosuoquan sag is smaller and the south slope zone of the Wulungu Depression is closed to the step-fault zone, the sedimentary centre is located between them, and there was no significant migration.

The sag-controlled fault did not break through the Cretaceous strata in all the profiles. However, the formations above the Cretaceous were involved in fold deformation to different degrees. Growth strata could be recognized in many profiles. In the *B*–*B*′ profile and the *C*–*C*′ profile (Figs. 6 and 7), The Cretaceous strata and the Cenozoic strata are growth strata, and a growth triangle zone is restricted by the antiformal axial surface (indicated in green colour) and the synformal axial surface (indicated in red colour). Denudation was widespread as the growth triangle zone was not closed. In the *D*–*D*′ profile (Fig. 8), there is also a growth triangle zone formed by the Cretaceous to Cenozoic strata, with the closing point located in the Cenozoic layer.

4.3. Characteristics of the Cretaceous–Paleogene strata

All the profiles indicate the presence of complex internal structures in the Cretaceous–Paleogene strata. We selected three profiles from the western, middle and eastern segments for detailed study.

In the western profile (Fig. 9a), 11 small layers are recognized in both the Cretaceous and the Paleogene. The base of the Cretaceous is an unconformity with truncations and onlap points near it. The K_2–K_6 events successively onlap onto the K_1 event, and K_8, K_9 also onlap onto the K_7 event. Strong onlap points could be observed above the base of Paleogene (E_1). In addition, the E_5 and E_9 events onlap onto the E_4 and E_8 events, respectively.

In the middle profile (Fig. 9b), the Cretaceous could be divided into 17 small layers (K_1–K_{17}), and the Paleogene has 10 small layers (E_1–E_{10}). Strong truncation can be observed along the base of the Cretaceous (K_1), particularly in the Hongyan step-fault zone and the Suosuoquan sag. The K_2 event is parallel to the K_1 event, and the

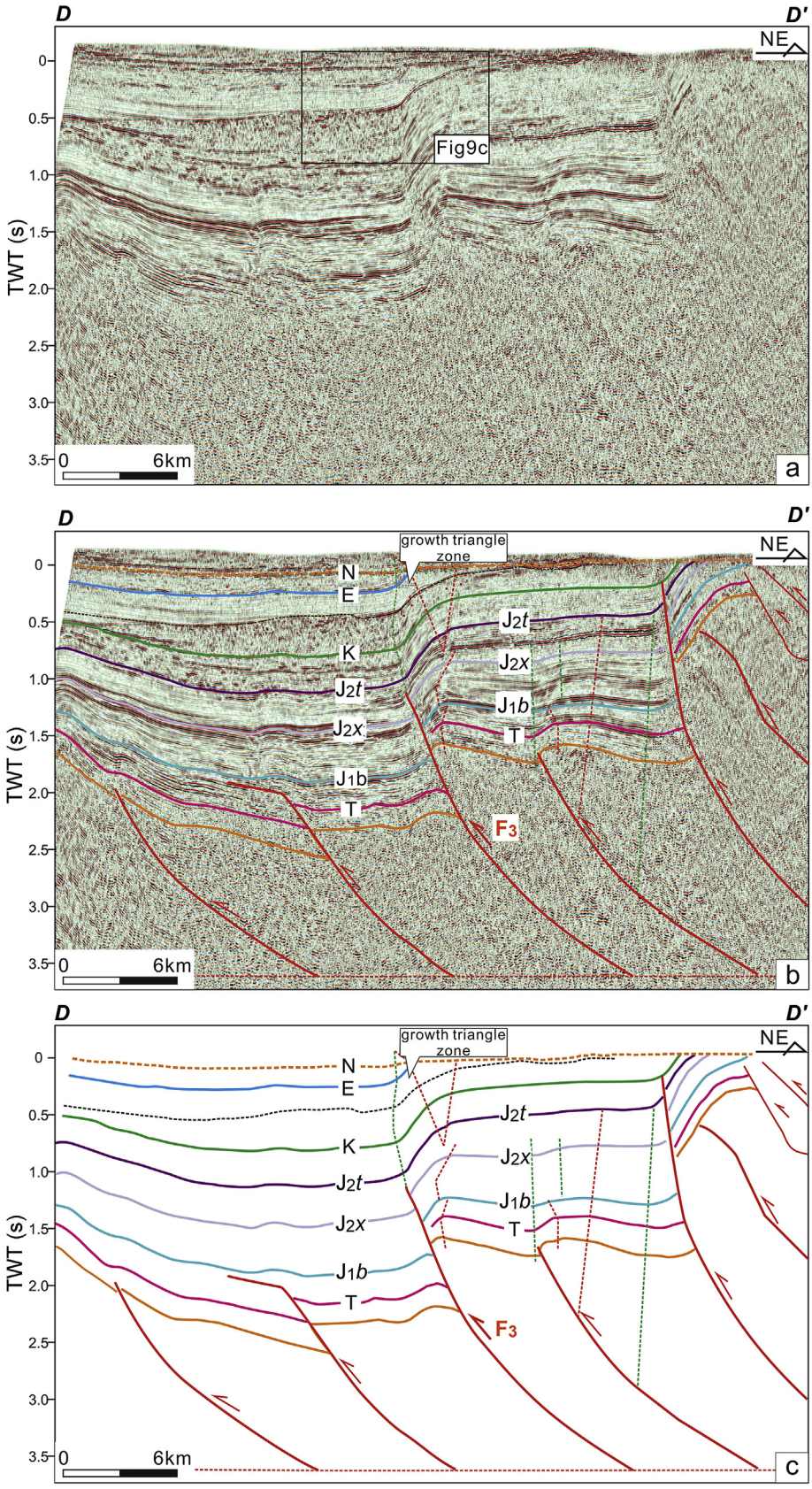

Figure 8. Seismic profile of *D*–*D*′. (a) Original profile of *D*–*D*′; (b) Interpreted profile of *D*–*D*′; (c) Pure interpreted profile of *D*–*D*′.

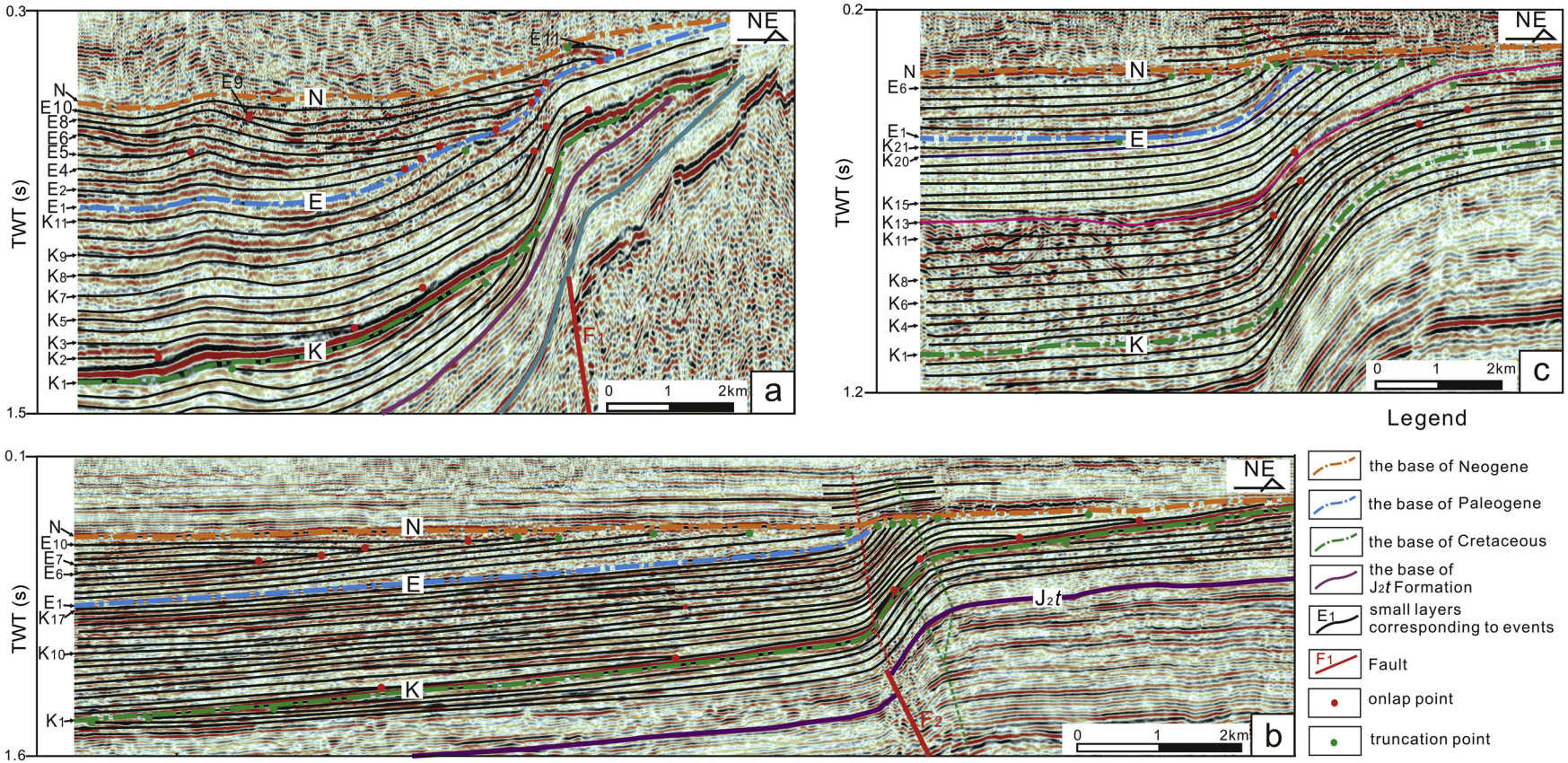

Figure 9. Interpreted profile showing the small layers. (a) Profile from the western profile (*A*–*A*′); (b) Profile from the middle profile (*B*–*B*′); (c) Profile from the eastern profile (*D*–*D*′).

K_3–K_8 events successively onlap onto the K_2 event. The K_9–K_{17} and E_1–E_6 are all truncated by the Neogene event except for the K_{11} event, which is a regressive offlap event that offlaps onto the K_{10} event. The E_7–E_{10} events onlap onto the K_6 event with no variation in width.

In the eastern profile (Fig. 9c), the Cretaceous strata could be divided into 21 small layers (K_1–K_{21}) and the Paleogene could be divided into six small layers (E_1–E_6). Visible truncated points can be observed along the base of the Cretaceous (K_1), particularly in the Hongyan step-fault zone. However, no overlap points exist above the base of the Cretaceous (K_1). The K_2–K_5 events are parallel to the K_1 event, the width between them does not vary from the edge to the interior of the basin. The K_6 event is an onlap surface, and the K_7 and K_8 events successively onlap onto the K_6 event. The K_9 event regressively offlaps onto the K_8 event, and the K_{10} event onlaps onto the K_8 event. The K_{13} event is a mini-unconformity with truncation points underneath, and the K_{14} event onlaps on the K_{13} event. The K_{15}–K_{20} events are all truncated by the Neogene event. The E_1 event is an unconformity truncating the K_{21} event; however the E_1–E_6 events are also successively truncated by the Neogene event.

5. Discussions

5.1. Timing of the reactivation

Three large regional unconformities have been developed in The Wulungu region since the Cretaceous, and the degree of denudation is relatively large near the transitional zone between the Suosuoquan sag and the Hongyan step-fault zone. In our opinion, this tectonic movement has occurred since the Cretaceous, with the relatively large-scale uplift near the step-fault zone being denuded. The sag-controlled fault at the edge of the step-fault zone, which developed since the Triassic, can control tectonic movement. In addition, the existence of growth strata also limited the active stage of the fault. Growth triangle zones could be recognized on all the profiles, which prove that the sag-controlled faults were reactivated after they formed.

Thus, together with the development of unconformities and the existing growth triangle zone, we have reasons to believe that the faults in the step-fault zone have experienced reactivation to different degrees since the Cretaceous.

5.2. Evolution since the Cretaceous

5.2.1. Western segment

The Cretaceous and Paleogene can both be divided into 11 small layers: K_1–K_{11} and E_1–E_{11}, respectively (Fig. 10a–l). Before formation of the Cretaceous regional unconformity, two uplifts existed in the transition and the Suosuoquan sag. These were eroded by the base of the Cretaceous, resulting in many truncation points. At the beginning of the Cretaceous, the Tuzituoyila Fault (F_1) recommenced thrusting, making the step-fault zone rise slightly. The depositional rate, however, was greater than the rate of tectonic uplift over the entire depression, and events occurred not only at the overlap at the basin edges, but were also involved in the fold caused by the thrusting of F_1 (Fig. 10b and c). When the K_7 sequence was formed, the overlap phenomenon ceased, resulting in stratigraphical sedimentary cover to the step-fault zone (Fig. 10d). However, after deposition of K_7, the step-fault zone was rapidly uplifted, outpacing the depositional rate. Offlap points can be seen on the seismic profile (Fig. 10e, K_8 seismic event). But immediately after the short-term offlap, there was a reoccurrence of onlap (Fig. 10e and f). During the Cretaceous period, the uplift rate of the step-fault zone was generally small, with rapid uplift in the medium term.

Before the formation of the Paleogene unconformity, a construction highness existed in the transitional zone caused by the reactivity of F_1 (Fig. 10g). This was eroded by the base of Paleogene, forming many truncation points. The Paleogene, together with the lower layers of the Cretaceous strata, subsequently tilted significantly (about 15°) towards to the basin (Fig. 10h and i). However, the sequence was still onlapping from the basin to the step-fault zone. Therefore, the rate of deposition remained comparatively greater than the rate of uplift. Prior to the sedimentary layer E_{10}, an uplift was formed in the sag, indicating that two uplifts were present in the sag and the step-fault zone in the profile. It is easy to determine that the E_9 seismic event onlapped onto the two uplifts at the same time (Fig. 10j). Subsequently, both sides of the uplift continued to be active, and were truncated by the bottom boundary of the Neogene. Deformation during the whole Paleogene was mainly tilted at a large angle to the basin. Meanwhile, an uplift formed in the Suosuoquan sag.

The length of the A–A' profile from the western segment at present is 15.08 km. The length before deposition of the Cretaceous strata, however, was 17.64 km, making the shortening length 2.56 km and the shortening rate 14.5%.

5.2.2. Middle segment

The Cretaceous can be divided into 17 small layers in the middle segment (K_1–K_{17}). Overall, the characteristics of the small layers are very similar to those of the western segment (Fig. 11a–g): a large-scale onlap phenomenon at the beginning of the Cretaceous (Fig. 11b) and a K_2 event parallel to the base of the Cretaceous. However, the K_3–K_9 seismic events were onlap onto the K_2 event. A short-term offlap appeared (Fig. 11c) during which the K_{10} seismic event covered the step-fault zone and the K_{11} seismic event was deposited into the Suosuoquan sag with offlap phenomenon. Subsequent Cretaceous layers (K_{12}–K_{17}) with growth strata covered the entire region.

The Paleogene can be divided into 10 small layers (E_1–E_{10}). Truncation points under the base of the Paleogene are predominantly present in the transition and step-fault zones, making these two places construction highnesses prior to the formation of the unconformity. The E_2 and E_3 events were then onlap onto the unconformity. The width between the two events did not change from the basin to the step-fault zone, suggesting that they were caused by sea level change. Subsequent, seismic events have covered the entire area, and have been involved in the folding caused by the reactivity of fault (Fig. 11d). After the E_6 event, similarly to the western profile, the fault experienced a large-scale thrust movement which titled (about 5°) the E_7 and underlying layers towards the basin (Fig. 11e). E_7 was an offlapping seismic event, whereas the other events in the sag after E_6 were all onlapping. However, the width between E_7 and E_{10} events was stable (Fig. 11f), making it obvious that the South Lun-2 Fault (F_2), following the large angular tilt, experienced a stable period during which tectonic movement almost ceased. Meanwhile, the sequence above the E_6 event, which was located in the construction highness, was denuded and displayed many truncation points.

The length of the B–B' profile from the middle segment at present is 9.87 km, while the length before deposition of the Cretaceous strata was 10.94 km, indicating a shortening length of 1.07 km and a shortening rate of 9.8%.

5.2.3. Eastern segment

The structure of the Cretaceous strata in the eastern profile is relatively complex, and can be divided into 21 small layers (K_1–K_{21}) (Fig. 12a–k). The step-fault zone was a construction highness prior to the formation of the base of the Cretaceous (K_1), which was denuded by the Cretaceous unconformity (Fig. 12a). The sag-

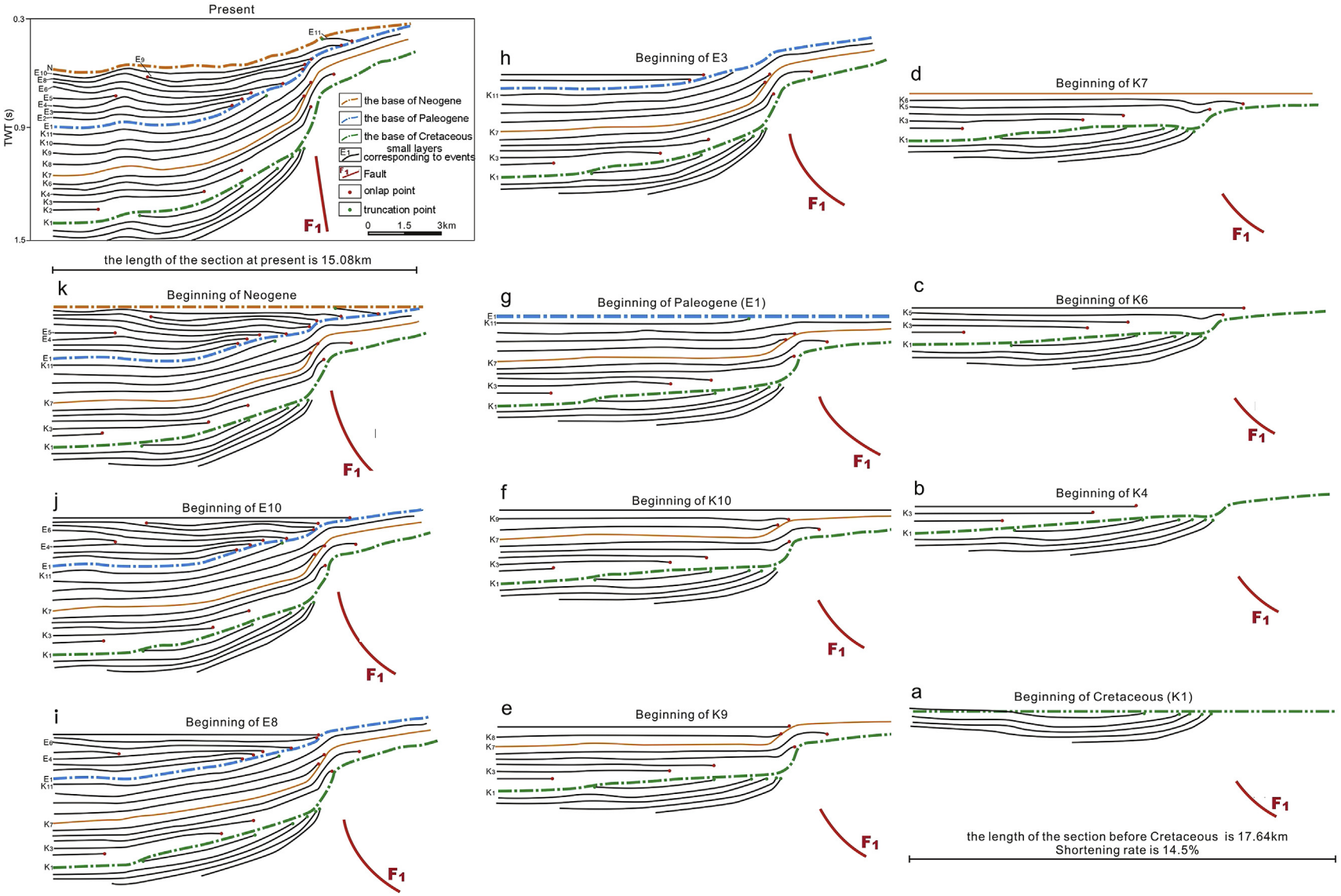

Figure 10. The tectonic evolution of the small layers since the Cretaceous from the western profile (*A*–*A*′).

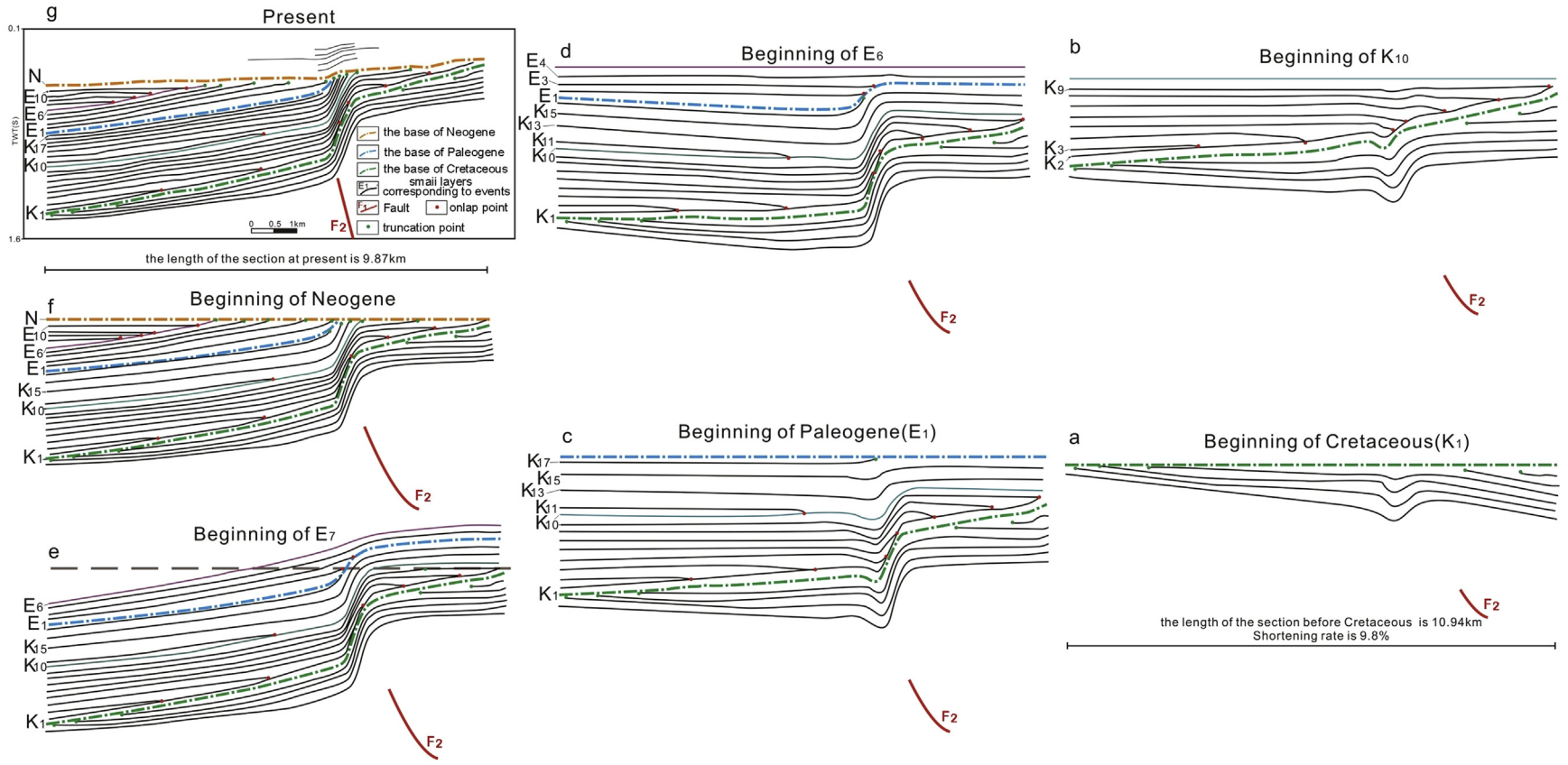

Figure 11. The tectonic evolution of the small layers since the Cretaceous from the middle profile (*B*–*B*′).

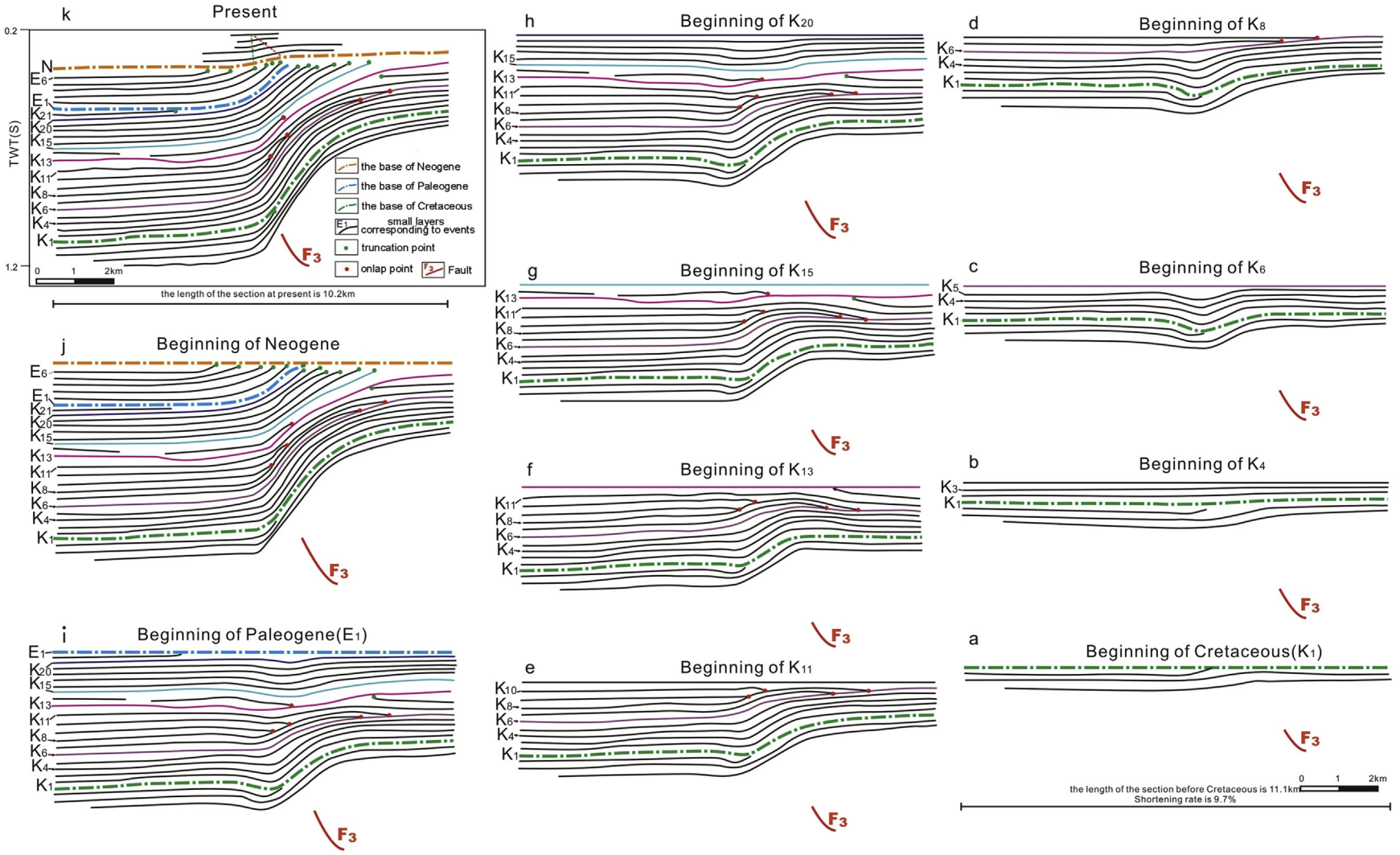

Figure 12. The tectonic evolution of the small layers since the Cretaceous from the eastern profile (*D*–*D*′).

controlled fault (F_3) was not reactivated during the sedimentation of K_2–K_5 intervals (Fig. 12b). At the beginning of the K_6 interval, the Hongpen Fault (F_3) commenced its reactivity. With the reactivation of F_3, the early depositional layers (K_2–K_5) above the unconformity were involved in the flexural deformation. Alternatively the sequences formed at a later period were syndepositional deformation (Fig. 12c and d). The sedimentary centre was located in the sag behind the step-fault zone. The thickness of the strata in the sag was obviously greater than that of the strata within the step-fault zone. After deposition of the K_6 interval, the K_7 event experienced obvious offlap relative to K_6, illustrating that the uplift rate caused by the thrust of the Hongpen Fault (F_3) was high relative to the sedimentation rate. The widespread overlap subsequently occurred towards the step-fault zone along K_6 (Fig. 12d). K_8 and K_9 represented a similar offlap and onlap cycle. However, overlap events also were involved in the folding, and as such it is obvious that the thrust reactivity of the fault did not cease with the occurrence of overlap. However, the effect of thrust was weak, with the uplift rate being less than the deposition rate. The K_{13} seismic event was a small erosion surface. It is obvious that many denudation points exist under this surface and many onlap points are present above the surface. This surface denuded the small uplift caused by the fault reactivity (Fig. 12f).

The Paleogene can be divided into six small layers (E_1–E_6). Movement during the Paleogene was relatively simple. The E_2–E_5 events were synsedimentary sequences, with a small movement rate. However during the deposition of E_6, the fault experienced large-scale thrust reactivity, causing rapid uplift of the Cretaceous–Paleogene strata and denudation of sequences by the Neogene unconformity surface. Denudation points spread over the sag and step-fault zone.

The length of the D–D' profile from the eastern segment at present is 10.2 km, while the length before deposition of the Cretaceous strata was 11.1 km, indicating a shortening length of 0.9 km and a shortening rate of 9.7%.

5.2.4. Comparison among western, middle and eastern segments

Thrust reactivation in the Wulungu Depression was proved in all the profiles, and the shortening rate was about 10% in all cases. The visible thrust reactivation strength was high. In addition, the tectonic activity rate relative to the deposition rate changed and thrusting activities continued for a long time, continuing into the Cenozoic. Overall, the reactivation of thrusting represents a kind of episodic activity.

Reactivation in different segments of the Wulungu Depression showed certain differences, such as the difference in the timing of thrust reactivation. In the western and middle segments, thrust reactivation began in the Cretaceous, with widespread onlapping seismic events related to the tectonic activity on the Cretaceous unconformity; while the reactivation time of the eastern segment was relatively late, with no onlapping seismic events visible on the Cretaceous unconformity surface. The strength of reactivation also varied slightly: the shortening rate was higher in the western segment than in the other segments. Additionally, the reactivation of the western segment was also relatively strong.

5.3. The geometric model

The sag-controlled fault located in the Hongyan step-fault zone, shows a type of fault-propagation folding. These can be divided into several types: constant thickness fault-propagation folds and fixed-axis fault-propagation folds (Suppe and Medwedeff, 1990), basement-involved (drape) folding with migrating triple junctions (Narr and Suppe, 1994) and trishear fault-propagation folds (Erslev, 1991; Allmendinger, 1998).

Basement-involved folds commonly have six general characteristics (Narr and Suppe, 1994): (1) they are often monoclines; (2) the structures commonly form above a contractional fault in the basement; (3) the main fault can disappear as it proceeds up into the cover sequence; (4) the basement behaves as a rigid block in some structures, but is folded in others; (5) the steep limbs of folds are commonly formed by the cover draping over a faulted edge of basement as the hanging wall is uplifted; (6) deformation in the cover is concentrated in the steep limb and can involve both layer-parallel shortening and layer-parallel extension.

Basement faults spread upward into the sedimentary cover, because of the differences in rheological properties between the basement and the cover. They often have a strong brittle fracture deformation zone in the basement and are replaced by a widening-upwards triangular deformation zone in the sedimentary cover. The vertex of the triangle is fixed at the endpoint of the fault. As the fault endpoint propagates forwards, the triangular deformation zone constantly moves forwards. For this type of force fold associated with basal faulting, Erslev (1991) put forward the concept of triangular shear folding and a kinematical model to describe the geometry.

From the profiles in the Wulungu Depression, it is the authors' opinion that the research area displays a basement involved fold mechanism linked with triangular shear folding. The basement is the Palaeozoic rocks and the Mesozoic–Cenozoic strata are involved in the deformation as the cover layers (Fig. 13a and b). Specifically, the main fault broke through the basement and entered the Jurassic strata prior to the events associated with the basement-involved structures during Mesozoic and Cenozoic time. In order to build an evolutionary model of the triangular shear folding, six parameters are required: the fault ramp angle, the slip, the propagation/slip (P/S), the trishear angle and the location of the fault tip. This paper chose FaultFoldForward, founded by Richard W. Allmendinger and 2D-Move, as the basic instrument for constructing the evolutionary model.

In the B–B' depth profile (Fig. 13b), the initial fault tip was at A and the fault tip is located at present at B. The total propagation (Ps) is 4940 m, the fault ramp angle (θ) is about 60° and the trishear angle (Φ) is 60°. The fault slip in the Triassic strata (S_T) is 1600 m (Fig. 13b). However, the slip will be greater closer to the fault tip; the initial fault tip is deeper than T, and therefore, the total slip (S) must be greater than 1600 m. The P/S value should be less than 3.0. The elevation difference for the different layers between the footwall and the hanging wall can be calculated from the profile: ΔN = 140 m, ΔE = 420 m, ΔK = 750 m, ΔJ_2t = 1160 m, ΔJ_2x = 1450 m, ΔJ_1b = 1570 m and ΔT = 2000 m. The various periods of uplift can be calculated using inversion: T ($\Delta T - \Delta J_1b$) = 430 m, J_1b ($\Delta J_1b - \Delta J_2x$) = 120 m, J_2x ($\Delta J_2x - \Delta J_2t$) = 290 m, J_2t ($\Delta J_2t - \Delta K$) = 410 m, K ($\Delta K - \Delta E$) = 330 m, E ($\Delta E - \Delta N$) = 280 m and N (ΔN) = 140 m. Simulations can then be conducted by selecting different values of P/S and combining them with the calculated parameters. The simulations showed that the slip during each period had no relationship to the P/S, but was affected by the elevation difference: ΔS_T = 500 m, ΔS_{J_1b} = 140 m, ΔS_{J_2x} = 340 m, ΔS_{J_2t} = 480 m, ΔS_K = 380 m, ΔS_E = 320 m and ΔS_N = 160 m. Thus, the total slip (S_{total}) is 2320 m and the P/S is 2.1. The evolutionary parameters during various periods have been obtained (Fig. 14).

As the proposed analysis was performed using the trishear model, its accuracy depends on whether the trishear model is representative of the actual deformation. Moreover, the proposed trishear model was based on these assumptions: (1) the ramp angle of the fault and the P/S ratio remained constant during all fault propagation events; and (2) the apical angles along both sides of the fault line are equal and did not change for all fault propagation

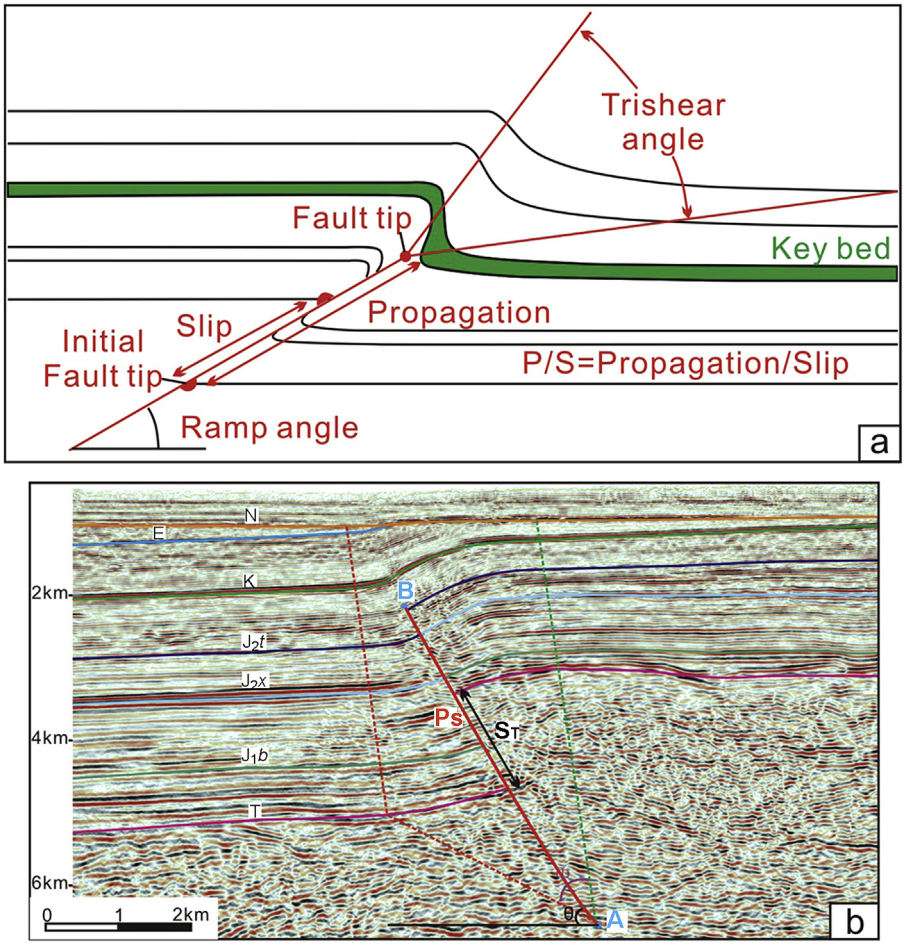

Figure 13. (a) Theoretical model of Triangle Shear Fold; (b) Depth seismic profile from B–B': Φ—Trishear angle, θ—Fault ramp angle, Ps—The total propagation, S_T—The fault slip in the Triassic, A—Initial fault tip, B—Fault tip.

events. These assumptions will invariably differ from reality (see for example a comparison of the results from the sandbox and the trishear model; Lin et al., 2006). Due to the variety of different lithologies present, the trishear angle (Φ) will be different in the different strata. Therefore, the inferred fault propagation history will also differ from the actual propagation history. Further work to evaluate this discrepancy is necessary.

5.4. Tectonic implications

The presence of thrusting in the northern Junggar Basin since the Mesozoic–Cenozoic has been recognized by many scholars. Shi (2002) believed that the northern margin of the Junggar Basin experienced two stages of thrust movement during the Paleogene. The first movement started in the Palaeocene and ended in the Eocene. The basal fault experienced a strong thrust reactivation and a thick layer of coarse clastic sediments, mostly sandy fan and gravel fan, formed in the front of the fault. At the same time, river alluvial plain sediment and local underwater gravity flow deposits developed in places far away from the faults. The second period of activity occurred during the Eocene and Oligocene. During this period, uplift of the mountains of northern Xinjiang recommenced and strong thrust activity again occurred in the northern faults. Coarse clastic sediment and underwater gravity flow deposits formed in the front edge and distal area of the thrust belt, respectively. These two thrust relativities, resulting from the movement of the Tuzituoyila Fault, were intermittent and discontinuous.

Chen et al. (2011) established a four-stage sedimentary-tectonic evolution model for the northern Junggar Basin during the late Cenozoic based on a reconstruction of the sedimentary filling processes and the Cenozoic tectonic movements. Stage 1 (Palaeocene–Eocene) corresponds to the Honglishan Formation, which unconformably overlies the lower units. In stage 2 (Eocene–Oligocene), the tectonic movement in the early part of the Eocene, corresponding to the beginning of the Ulunguhe Formation deposition, caused a new stage of mountain uplift in northern Xinjiang and thrusting along the northern boundary faults of the basin (Peng, 1998; Yuan et al., 2006). This led to erosion of the upper part of the Honglishan Formation. Stage 3 occurred from the late Miocene to the middle Pleistocene. In stage 4 (late Pleistocene to the present), most parts of the northern Junggar Basin probably re-subsided during the late Pleistocene and were filled by the Xinjiang conglomerates. The basin was again slightly uplifted after the late Pleistocene in response to thrust and strike-slip deformation along the Irtysh fault system in the north (Bai, 1996), along the southern front of the Altai Mountains, and normal and right-lateral strike-slip faulting along the Keketuohai–Ertai Fault to the northeast (Shen et al., 2003).

Previous studies on thrusting after the Mesozoic–Cenozoic along the northern Junggar Basin have all involved the study of sedimentary response, but have rarely recognized thrusting from seismic profiles, which can directly reflect structural deformation. This study could make up for the deficiencies of previous studies. This research shows that sag-controlled faults of the Wulungu

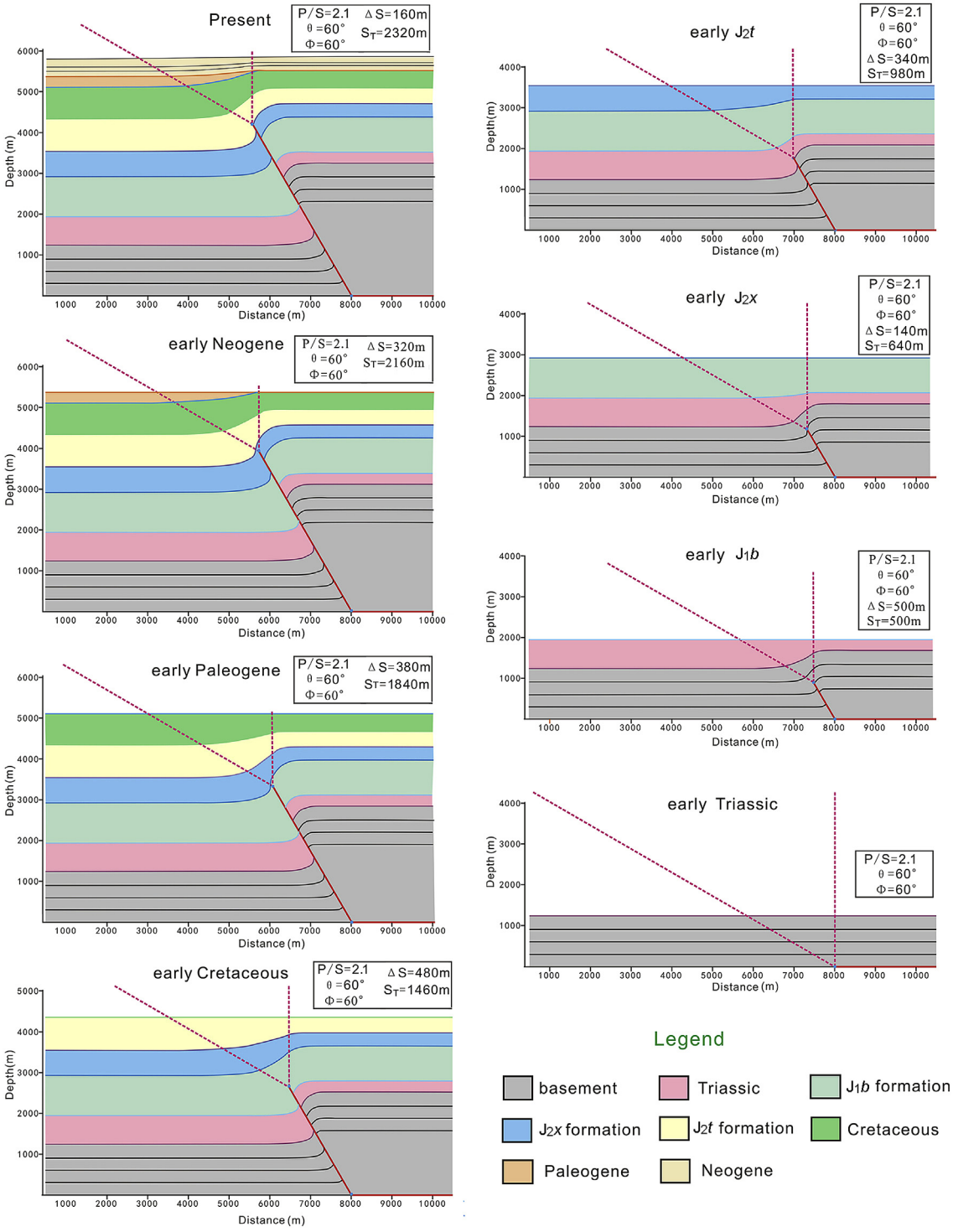

Figure 14. The forward model with the optimum set of trishear fit parameters.

Depression along the northern margin of the Junggar Basin have experienced thrust reactivity to different degrees since the late Mesozoic. The thrust faulting is from the basement, in combination with triangular shear folding. The thrusting lasted for a long time, possibly continuing into the Cenozoic. Overall there was reactivation of episodic activity.

Mesozoic–Cenozoic deformation in the northern Xinjiang area consisted of the following: (1) strong uplift and erosion of the rejuvenated Tianshan Mountains, the Altai Mountains, and the West and East Junggar terranes (Deng et al., 1999; Guo et al., 2006; Yuan et al., 2006; Li et al., 2008); (2) well-developed thrusting and thrust-related folds in the Mesozoic–Cenozoic depression in coupled areas of the Junggar Basin with the Tianshan Mountains (Deng et al., 1999; Guo et al., 2006, 2007; Chen et al., 2009); (3) basement-related thrusting in the front of the Bogda Mountains (Peng et al., 1990; Chen et al., 2007; Yang et al., 2008); (4) sinistral

strike-slip along the Da'erbute Fault in West Junggar, dextral strike-slip and earthquake movement along the Ertai–Keketuohai Fault in the northeast (Shen et al., 2003); and (5) thrusting and strike-slip movement along the Irtysh Fault at the northern margin of the Junggar Basin (Bai, 1996).

Field evidence and ESR-dating suggest that the regional deformations were NS-trending with shortening in the middle Pleistocene. Previous data have shown that the intercontinental convergence between the Indian and Asian blocks played an important role in the construction of the landforms and the deformation in the Xinjiang area, NW China, during the Cenozoic. This indicates that the direction of regional compressional stress should trend south–north, with northward descent of Cenozoic tectonic movement (Guo et al., 2006; Chen et al., 2009).

The Mesozoic deformation of Northern Xinjiang may be related to the closure of the palaeo-Tethys (Roger et al., 2010) and the related collisions of peri-Gondwanan continental fragments (so-called Cimmerian blocks) at the Tethyan margin, south of the Altai–Sayan region (Davies et al., 2010). Furthermore, tectonic activity was accompanied by the emplacement of a limited number of Triassic–Jurassic intra-plate intrusions across the entire Altai basement and tectonic terrane boundaries (Pirajno, 2010; Glorie et al., 2011). During the late Cretaceous and early Paleogene, continued Tethyan subduction eventually contributed to major India-Eurasia continent–continent collision at the Mesozoic–Cenozoic transition. This collision and the ongoing convergence between both continents have dominated Asian tectonic evolution ever since. The Altai Mountains were subjected to late Cenozoic reactivation as a response to the continued indentation of India into Eurasia (Dobretsov et al., 1996) and represent an active transpressional belt between the rigid Junggar and the Kazakhstan basement (southwest) and Siberia and Mongolia (northeast). That the tectonic regime is transpressional is demonstrated by the strike-slip and thrust movement along major faults (e.g. the Irtysh Fault Zone) (Buslov et al., 1999). This type of thrust reactivation of basal faults can also be seen in the Wulungu Depression of the Junggar Basin.

6. Conclusions

The faults in the step-fault zone of the northern margin of the Junggar Basin have experienced reactivity to different degrees since the Cretaceous. This represents episodic reactivation.

The shortening rate for all profiles was about 10%. The reactivation differed for various segments of the Wulungu Depression.

The thrust faulting is basement-involved, in combination with triangular shear folding. Thrusting lasted for a long time and continued into the Cenozoic.

Acknowledgements

Constructive reviews and suggestions by Wenjiao Xiao and two anonymous reviewers and the editorial suggestion of M. Santosh helped to improve the revised version. This research was financially supported by the National Science and Technology Major Project (No. 2011ZX05008-001), the Natural Science Foundation of China (No. 40739906), and the Chinese State 973 Project (No. 2011CB201100).

References

Allmendinger, R.W., 1998. Inverse and forward numerical modeling of trishear fault-propagation folds. Tectonics 17, 640–656.
Anadón, P., Cabrera, L., Colombo, F., Marzo, M., Riba, O., 1986. Syntectonic intraformational unconformities in alluvial fan deposits, eastern Ebro Basin margins (NE Spain). In: Allen, P.A., Homewood, P. (Eds.), Foreland Basins. International Association of Sedimentologists Special Publication, vol. 8. Blackwell, Oxford, pp. 259–271.
Anastasio, D.J., Erslev, E.A., Fisher, D.M. (Eds.), 1997. Fault-Related Folding. Journal of Structural Geology, Special Issue, vol. 19, pp. 3–4 (v–vi).
Bai, M.X., 1996. Ertix active fault zone. Xinjiang Geology 14, 127–134 (in Chinese with English abstract).
Baranoski, M.T., Dean, S.L., Wicks, J.L., Brown, V.M., 2009. Unconformity-bounded seismic reflection sequences define Grenville-age rift system and foreland basins beneath the Phanerozoic in Ohio. Geosphere 5, 140–151.
Buslov, M.M., Zykin, V.S., Novikov, I.S., Delvaux, D., 1999. The Cenozoic history of the Chuya depression (Gorny Altai): structure and geodynamics. Geologiya i Geofizika 40, 1720–1736.
Butler, R.W.H., Lickorish, W.H., 1997. Using high-resolution stratigraphy to date fold and thrust activity: examples from the Neogene of south-central Sicily. Journal of the Geological Society (London) 154, 633–643.
Chen, S.P., Qi, J.F., Yu, F.S., Yang, Y.Q., 2007. Deformation characteristics in the southern margin of the Junggar basin and their controlling factors. Acta Geologica Sinica 81, 152–157 (in Chinese with English abstract).
Chen, Z.L., Lu, K.G., Wang, G., Chen, B.L., Li, L., Jiang, R.B., Cui, L.L., Gong, H.L., 2009. Characteristics of the Cenozoic deformation in basin/range coupling regions on both sides of Tianshan Mountains and its geodynamics. Earth Science Frontiers 16, 149–159 (in Chinese with English abstract).
Chen, Z.L., Liu, J., Gong, H.L., Han, F.B., Briggs, S.M., Zheng, E.J., Wang, G., 2011. Late Cenozoic tectonic activity and its significance in the Northern Junggar Basin, Northwestern China. Tectonophysics 497, 45–56.
Choulet, F., Chen, Y., Wang, B., Faure, M., Cluzel, D., Charvet, J., Lin, W., Xu, B., 2011. Late Paleozoic paleogeographic reconstruction of Western Central Asia based upon paleomagnetic data and its geodynamic implications. Journal of Asian Earth Sciences 42, 867–884.
Coakley, B., Watts, J., Coakley, A., Watts, B., 1991. Tectonic controls on the development of unconformities: the North Slope, Alaska. Tectonics 10, 101–130.
Coleman, R.G., 1989. Continental growth of northwest China. Tectonics 8, 621–635.
Davies, C., Allen, M.B., Buslov, M.M., Safonova, I., 2010. Deposition in the Kuznetsk Basin, Siberia: insights into Permian–Triassic transition and the Mesozoic evolution of Central Asia. Palaeogeography, Palaeoclimatology, Palaeoecology 295, 307–322.
De Grave, J., Buslov, M.M., Van den Haute, P., 2007a. Distant effects of India–Eurasia convergence and Mesozoic intracontinental deformation in Central Asia: constraints from apatite fission-track thermochronology. Journal of Asian Earth Sciences 29, 188–204.
De Grave, J., Buslov, M.M., Van den haute, P., Dehandschutter, B., Delvaux, D., 2007b. Meso-Cenozoic evolution of mountain range — intramontane basin systems in the Southern Siberian Altai Mountains by apatite fission-track thermochronology. In: Lacombe, O., Lavé, J., Roure, F., Vergés, J. (Eds.), Thrust Belts and Foreland Basins, Frontiers in Earth Sciences. Berlin Heidelberg, pp. 457–470.
De Grave, J., Buslov, M.M., Van den haute, P., Metcalf, J., Dehandschutter, B., McWilliams, M.O., 2009. Multi-method chronometry of the Teletskoye graben and its basement, Siberian Altai Mountains: new insights on its thermotectonic evolution. In: Lisker, F., Ventura, B., Glasmacher, U.A. (Eds.), Thermochronological Methods: From Palaeotemperature Constraints to Landscape Evolution Models. Geological Society, Special Publications, London, pp. 237–259.
Deng, Q.D., Feng, X.Y., Zhang, P.Z., Yang, X.P., Xu, X.W., Peng, S.Z., Li, J., 1999. Reverse fault and fold zone in the Urumuqi range-front depression of the northern Tianshan and its genetic mechanism. Earth Science Frontiers 6, 191–201 (in Chinese with English abstract).
Dickinson, J.A., Wallace, M.W., Holdgate, G.R., Gallagher, S.J., Thomas, L., 2002. Origin and timing of the Miocene–Pliocene unconformity in southeast Australia. Journal of Sedimentary Research 72 (2), 288–303.
Dobretsov, N.L., Buslov, M.M., Delvaux, D., Berzin, N.A., Ermikov, V.D., 1996. Meso- and Cenozoic tectonics of the Central Asian mountain belt: effects of lithospheric plate interaction and mantle plumes. International Geology Review 40, 430–466.
Erslev, E.A., 1991. Trishear fault-propagation folding. Geology 24, 617–620.
Ghiglione, M., Ramos, V.A., 2005. Progression of deformation and sedimentation in the southernmost Andes. Tectonophysics 405, 25–46.
Glorie, S., De Grave, J., Buslov, M.M., Zhimulev, F.I., Izmer, A., Vandoorne, W., Ryabinin, A., Van den Haute, P., Vanhaecke, F., Elburg, M.A., 2011. Formation and Palaeozoic evolution of the Gorny–Altai–Altai–Mongolia suture zone (South Siberia): zircon U/Pb constraints on the igneous record. Gondwana Research 20 (2–3), 465–484.
Guo, Z.J., Zhang, Z.C., Wu, C.D., Fang, S.H., Zhang, R., 2006. The Mesozoic and Cenozoic exhumation history of Tianshan and comparative studies to the Junggar and Altai Mountains. Acta Geologica Sinica 80, 1–15 (in Chinese with English abstract).
Guo, Z.J., Deng, S.T., Wei, G.Q., 2007. Comparative study of the foreland thrust belts of South and North Tianshan and implications for hydrocarbon accumulation. Earth Science Frontiers 14, 123–131 (in Chinese with English abstract).
Howard, J.P., Cunningham, W.D., Davies, S.J., Dijkstra, A.H., Badarch, G., 2003. The stratigraphic and structural evolution of the Dzereg Basin, western Mongolia: clastic sedimentation, transpressional faulting and basin destruction in an intraplate, intracontinental setting. Basin Research 15, 45–72.
Hummon, C., et al., 1994. Wilshire fault: earthquakes in Hollywood. Geology 22, 291–294.

Huuse, M., Clausen, O.R., 2001. Morphology and origin of major Cenozoic sequence boundaries in the eastern North Sea Basin: top Eocene, near-top Oligocene and the mid-Miocene unconformity. Basin Research 13 (1), 17–41.
Jahn, B.M., 2004. The central Asian orogenic belt and growth of the continental crust in the Phanerozoic. Journal of the Geological Society 226, 73–100.
Jahn, B.M., Wu, F.Y., Chen, B., 2000. Massive granitoid generation in Central Asian: Nd isotope evidence and implication for continental growth in the Phanerozoic. Episodes 23, 82–92.
Jaimes, E., de De Freitas, M., 2006. An Albian–Cenomanian unconformity in the northern Andes: evidence and tectonic significance. Journal of South American Earth Sciences 21, 466–492.
Jian, P., Liu, D.Y., Zhang, Q., Zhang, F.Q., Shi, Y.R., Shi, G.H., Zhang, L.Q., Tao, H., 2003. SHRIMP dating of ophiolite and leucocratic rocks within ophiolites. Earth Science Frontiers 10, 439–456 (in Chinese with English abstract).
Jolivet, M., Ritz, J.-F., Vassallo, R., Larroque, C., Braucher, R., Todbileg, M., Chauvet, A., Sue, C., Arnaud, N., De Vicente, R., Arzhanikova, A., Arzhanikov, S., 2007. Mongolial summits: an uplifted, flat, old but still preserved erosion surface. Geology 35, 871–874.
Jolivet, M., Dominguez, S., Charreau, J., Chen, Y., Li, Y., Wang, Q., 2010. Mesozoic and Cenozoic tectonic history of the central Chinese Tian Shan: reactivated tectonic structures and active deformation. Tectonics 29, TC6019.
Kovalenko, V.I., Yarmolyuk, V.V., Kovach, V.P., Kotov, V.P., Kozakov, I.K., Salnikova, E.B., Larin, A.M., 2004. Isotope provinces, mechanisms of generation and sources of the continental crust in the Central Asian mobile belt: geological and isotopic evidence. Journal of Asian Earth Sciences 23, 605–627.
Kröner, A., Windley, B.F., Badarch, G., Tomurtogoo, O., Hegner, E., Jahn, B.M., Gruschka, S., Khain, E.V., Demoux, A., Wingate, M.T.D., 2007. Accretionary growth and crustformation in the Central Asian Orogenic Belt and comparison with the Arabian-Nubian shield. In: Hatcher Jr., R.D., Carlson, M.P., McBride, H.H., Marínez Catalán, J.R. (Eds.), 4-D Framework of Continental Crust. Geological Society of America Memoir, 200, pp. 181–209.
Kröner, A., Kovach, V., Belousova, E., Hegner, E., Armstrong, R., Dolgopolova, A., Seltmann, R., Alexeiev, D.V., Hoffmann, J.E., Wong, J., Sun, M., Cai, K., Wang, T., Tong, Y., Wilde, S.A., Degtyarev, K.E., Rytsk, E., 2014. Reassessment of the continental growth during the accretionary history of the Central Asian Orogenic Belt. Gondwana Research 25, 103–125.
Li, Q., Simo, J.A., McGowran, B., Holbourn, A., 2004. The eustatic and tectonic origin of Neogene unconformities from the Great Australian Bight. Marine Geology 203, 57–81.
Li, L., Chen, Z.L., Qi, W.X., Wang, S.X., Chen, X.H., Wu, Y.P., Gong, H.L., Wei, X.C., Yang, Y., Li, X.Z., 2008. Apatite fission track evidence for uplifting-exhumation processes of mountains surrounding the Junggar Basin. Acta Petrologica Sinica 24, 1011–1020 (in Chinese with English abstract).
Li, D., He, D.F., Santosh, M., Tang, J.Y., 2013. Petrogenesis of Late Paleozoic volcanic from the Zhaheba depression, East Junggar: insights into collisional event in an accretionary orogen of Central Asia. Lithos 184–187, 167–193.
Lickorish, W.H., Ford, M., 1998. Sequential restoration of the external Alpine Digne thrust system, SE France, constrained by kinematic data and synorogenic sediments. In: Mascle, A., Puigdefábregas, C., Luterbacher, H.P., Fernández, M. (Eds.), Cenozoic Foreland Basins of Western Europe. Geological Society Special Publication, vol. 134. Geological Society, London, pp. 189–211.
Lin, M.L., Chung, C.F., Jeng, F.S., 2006. Deformation of overburden soil induced by thrust fault slip. Engineering Geology 88, 70–89.
Lin, C.S., et al., 2012. Distribution and erosion of the Paleozoic tectonic unconformities in the Tarim Basin, Northwest China: significance for the evolution of paleo-uplifts and tectonic geography during deformation. Journal of Asian Earth Sciences 46, 1–19.
Ma, C., Xiao, W.J., Windley, B.F., Zhao, G.P., Han, C.M., Zhang, J.E., Luo, J., Li, C., 2012. Tracing a subducted ridge-transform system in a late Carboniferous accretionary prism of the southern Altaids: orthogonal sanukitoid dyke swarms in Western Junggar, NW China. Lithos 140–141, 152–165.
Mascle, A., Puigdefábregas, C., Luterbacher, H.P., Fernández, M. (Eds.), 1998. Cenozoic Foreland Basins of Western Europe. Geological Society of London, Special Publication, vol. 134. Geological Society, London, 427 pp.
Medwedeff, D.A., 1989. Growth fault-bend folding at southeast Lost Hills, San Joaquin Valley, California. American Association of Petroleum Geologists Bulletin 73, 54–67.
Mindszenty, A., D'Argenio, B., Aiello, G., 1995. Lithospheric bulges recorded by regional unconformities. The case of mesozoic-tertiary apulia. Tectonophysics 252, 137–161.
Mount, V.S., Suppe, J., Hook, S.C., 1990. A forword modeling strategy for balancing cross-sections. American Association of Petroleum Geologists Bulletin 74, 521–531.
Narr, Wayne, Suppe, John, 1994. Kinematics of basement-involved compressive structures. American Journal of Science 294, 802–860.
Novoa, E., Suppe, J., Shaw, J.H., 2000. Inclined-shear restoration of growth folds. American Association of Petroleum Geologists Bulletin 84, 787–804.
Otonicar, B., 2007. Upper Cretaceous to Paleogene forebulge unconformity associated with foreland basin evolution (Kras, Matarsko Podolje and Istria; SW Slovenia and NW Croatia). Acat Carsologica 36, 101–120.
Paola, C., Domenico, C., 1995. Miocenen unconformity in the Central Apennines: geodynamic significance and sedimentary basin evolution. Tectonophysics 252, 375–389.
Peng, X.L., 1998. Appearance and characteristics of the Neotectonic movements in Xinjiang. Journal of Chengdu University Technology 25, 168–181 (in Chinese with English abstract).
Peng, X.L., Hu, B., Liu, L.J., 1990. A restudy for pre-Bogda mountain folded zone. Xinjiang Petroleum Geology 11, 276–295 (in Chinese with English abstract).
Ping, J., Dunyi, L., Yuruo, S., Fuqin, Z., 2005. SHRIMP dating of SSZ ophiolites from northern Xinjiang Province, China: implications for generation of oceanic crust in the Central Asian Orogenic Belt. IEC SB RAS, Irkutsk. In: Sklyarov, E.V. (Ed.), Structural and Tectonic Correlation across the Central Asia Orogenic Collage: North-Eastern Segment, Guidebook and Abstract Volume of the Siberian Workshop IGCP-480, p. 246.
Pirajno, F., 2010. Intracontinental strike-slip faults, associated magmatism, mineral systems and mantle dynamics: examples from NW China and Altay–Sayan (Siberia). Journal of Geodynamics 50, 325–346.
Rafini, S., Mercier, R., Eric, M., 2002. Forward modelling of foreland basins progressive unconformities. Sedimentary Geology 146, 75–89.
Ren, X.C., 2008. Tectonic unit division of Wulungu depression on Junggar Basin during Mesozoic. Petroleum Geophysics 6, 38–41 (in Chinese with English abstract).
Riba, O., 1989. Las discordancias sintectónicas como elementos de análisis de cuenca. Sedimentologia. Concejo Superior de Investigaciones Científicas, Madrid, pp. 489–522.
Roger, F., Jolivet, M., Malavieille, J., 2010. The tectonic evolution of the Songpan-Garze (North Tibet) and adjacent areas from Proterozoic to Present: a synthesis. Journal of Asian Earth Sciences 39, 254–296.
Safonova, I.Y., Utsunomiya, A., Kojima, S., Nakae, S., Tomurtogoo, O., Filippov, A.N., Koizumi, K., 2009. Pacific superplume-related oceanic basalts hosted by accretionary complexes of Central Asia, Russian Far East and Japan. Gondwana Research 16, 587–608.
Safonova, I.Y., Sennikov, N.V., Komiya, T., Bychkova, Y.V., Kurganskaya, E.V., 2011. Geochemical diversity in oceanic basalts hosted by the Zasur'ya accretionary complex, NW Russion Altai, Central Asia: implications from trace elements and Nd isotopes. Journal of Asian Earth Sciences 42, 191–207.
Şengör, A.M.C., Natal'in, B.A., Burtman, V.S., 1993. Evolution of the Altaid tectonic collage and Palaeozoic crustal growth in Eurasia. Nature 364, 299–307.
Shaw, J.H., Suppe, J., 1994. Active faulting and growth folding in the eastern Santa Barbara Channel, California. Geological Society of America Bulletin 106, 607–626.
Shen, J., Li, Y.Z., Wang, Y.P., Song, F.M., 2003. The active faults in Altai Mountains. Earth Science Frontiers 10 (Suppl.), 132–141 (in Chinese with English abstract).
Shen, X.M., Zhang, H.X., Ma, L., 2013. Zircon U-Pb and Amphibole $^{40}Ar/^{39}Ar$ geochronology of Kuert Ophiolite in Altay and geological implication. Journal of Guilin University of Technology 33, 394–405 (in Chinese with English abstract).
Shi, Z.L., 2002. Compressional and thrust structures of the Early Paleogene and their coupling sedimentary processes in the northern Junggar basin of Xinjiang. Xinjiang Geology 20, 115–117 (in Chinese with English abstract).
Souter, B.J., Hager, B.H., 1997. Fault propagation fold growth during the 1994 Northridge, California, earthquake. Journal of Geophysical Research 102, 11931–11942.
Suppe, J., Medwedeff, D.A., 1990. Geometry and kinematics of fault-propagation folding. Ecoglae Geologicae Helvetiae 83, 409–454.
Suppe, J., Chou, G.T., Hook, S.C., 1992. Rates of folding and faulting determined from growth strata. In: McClay, K.R. (Ed.), Thrust Tectonics. Chapman & Hall, Suffolk, pp. 105–121.
Tang, H.F., Su, Y.P., Liu, C.Q., Hou, G.S., Wang, Y.B., 2007. Zircon U-Pb age of the Plagiogranite in Kalameili belt, Northern Xinjiang and its tectonic implications. Geotectonica et Metallogenia 31, 110–117 (in Chinese with English abstract).
Vassallo, R., Jolivet, M., Ritz, J.-F., Braucher, R., Larroque, C., Sue, C., Todbileg, M., Javkhlanbold, D., 2007. Uplift age and rates of the Gurvan Bogd system (Gobi-Altay) by apatite fission track analysis. Earth and Planetary Science Letters 259, 333–346.
Wang, B.Y., Jiang, C.Y., Li, Y.J., Wu, H.E., Xia, Z.D., Lu, R.H., 2009. Geochemistry and tectonic implications of Karamaili ophiolite in East Junggar of Xinjiang. Journal of Mineralogy and Peteology 29, 74–82 (in Chinese with English abstract).
Windley, B.F., Alexeiev, D., Xiao, W.J., Kroner, A., Badarch, G., 2007. Tectonic models for accretion of the Central Asian Orogenic Belt. Journal of the Geological Society 164, 31–47.
Xiao, W.J., Kusky, T.M., 2009. Geodynamic processes and metallogenesis of the Central Asian and related orogenic belts: introduction. Gondwana Research 16, 167–169.
Xiao, W.J., Santosh, M., 2014. The western Central Asian Orogenic Belt: a window to accretionary orogenesis and continental growth. Gondwana Research 25, 1429–1444.
Xiao, W.J., Windley, B.F., Yan, Q.R., Qin, K.Z., Chen, H.L., Yuan, C., Sun, M., Li, J.L., Sun, S., 2006. SHRIMP zircon age of the Aermantai ophiolite in the north Xinjiang, China, and its tectonic implications. Acta Geologica Sinica 80, 32–36.
Xiao, W.J., Windley, B.F., Huang, B.C., Han, C.M., Yuan, C., Chen, H.L., Sun, S., Li, J.L., 2009. End-Permian to mid-Triassic termination of the accretionary processes of the southern Altaids: implications for the geodynamic evolution, Phanerozoic continental growth, and metallogeny of Central Asia. International Journal of Earth Sciences 98, 1189–1287.
Xiao, W.J., Huang, B., Han, C., Sun, S., Li, J., 2010. A review of the western part of the Altaids: a key to understand the architecture of accretionary orogens. Gondwana Research 18, 253–273.
Xiao, W.J., Windley, B.F., Allen, M., Han, C.M., 2013. Paleozoic multiple accretionary and collisional tectonics of the Chinese Tianshan orogenic collage. Gondwana Research 23, 1316–1341.

Xiao, W.J., Han, C.M., Liu, W., Wan, B., Zhang, J.E., Ao, S.J., Zhang, Z.Y., Song, D.F., Tian, Z.H., Luo, J., 2014. How many sutures in the southern Central Orogenic Belt insights from East Xinjiang-West Gansu (NW China)? Geosciences Frontiers 5 (4), 525–536.

Yang, X.P., Deng, Q.D., Zhang, P.Z., 2008. Crustal shortening of major nappe structures of the front margins of the Tianshan. Seismology Geology 30, 111–130 (in Chinese).

Yu, H.S., Chou, Y.W., 2001. Characteristics and development of the flexural forebulge and basal unconformity of Western Taiwan Foreland basin. Tectonophysics 333, 277–291.

Yuan, W.M., Carter, A., Dong, J.Q., Bao, Z., An, Y., Guo, Z., 2006. Mesozoic-Tertiary exhumation history of the Altai Mountains, northern Xinjiang, China: new constraints from apatite fission track data. Tectonophysics 412, 183–193.

Zapata, T., Allmendinger, R.W., 1996. Growth stratal records of instantaneous and progressive limb rotation in the Precordillera thrust belt and Bermejo basin, Argentina. Tectonics 15, 1065–1083.

Zhang, Y.Y., Guo, Z.J., 2010. New constraints on formation ages of Ophiolites in northern Junggar and comparative study on their connection. Acta Petrologica Sinica 26, 421–430 (in Chinese with English abstract).

Zhang, H.X., Niu, H.C., Terada, K., Yu, X.Y., Sato, H., Ito, J., 2003. Zircon SHRIMP U-Pb dating on plagiogranite from the Kuerti ophiolite in Altay, north Xinjiang. Chinese Science Bulletin 48, 2231–2235.

Zhang, Z.C., Mao, J.W., Cai, J.H., Kusky, T.M., Zhou, G., Yan, S.H., Zhao, L., 2008. Geochemistry of picrites and associated lavas of a Devonian island arc in the northern Junggar terrane, Xinjiang (NW China): implications for petrogenesis, arc mantle sources and tectonic setting. Lithos 105, 379–395.

Zoetemeijer, R., Sassi, W., Roure, F., Cloetingh, S., 1992. Stratigraphic and kinematic modeling of thrust evolution, northern Apennines, Italy. Geology 20, 1035–1038.